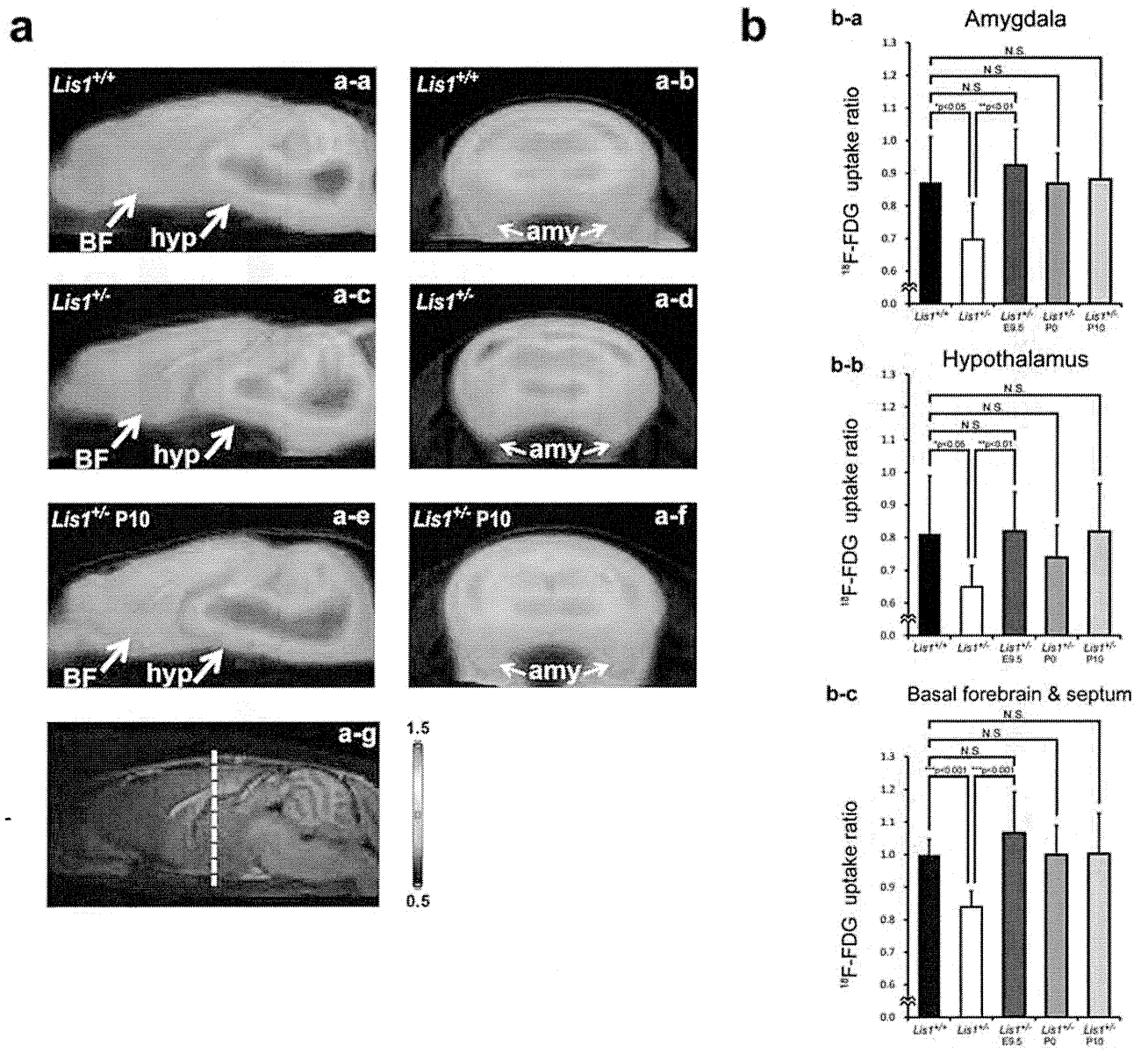

Figure 4 | Brain metabolism: ^{18}F-FDG PET scanning. *In vivo* ^{18}F-FDG-PET images and surface renderings of wild type (WT) mice and *Lis1*$^{+/-}$ mice are depicted. (a) Co-registration of microPET and MRI images obtained from WT mice (a-a, b) or *Lis1*$^{+/-}$ mice (a-c, d, e, f). The basal forebrain and hypothalamus are indicated by white arrows in sagittal images (BF, basal forebrain; hyp, hypothalamus) and amygdala is indicated by white arrows in coronal images (amy, amygdala). The location of coronal slice images is indicated as a white dash line in the sagittal MR image (a-g). Graded 2D slice images demonstrate the reduction of ^{18}F-FDG uptake in the basal forebrain, hypothalamus and amygdala of *Lis1*$^{+/-}$ mice (a-c, d). The color bar indicates normalized ^{18}F-FDG uptake ratio. (b) Quantification of ^{18}F-FDG uptake in several brain regions of each experimental group (*Lis1*$^{+/+}$; *Lis1*$^{+/+}$ mice without treatment (n = 8), *Lis1*$^{+/-}$; *Lis1*$^{+/-}$ mice without treatment (n = 8), *Lis1*$^{+/-}$E9.5; *Lis1*$^{+/-}$ mice with SNJ1945 treatment from E9.5 (n = 6), *Lis1*$^{+/-}$P0; *Lis1*$^{+/-}$ mice with SNJ1945 treatment from peri-natal period (n = 7) *Lis1*$^{+/-}$P10; Lis1$^{+/-}$ mice with SNJ1945 treatment from ten days after birth (n = 6)). Statistical examination was performed by unpaired Student's *t*-test. Values in graphs were expressed as mean ± SEM. Statistical significance was defined as *P < 0.05, **P < 0.01 and ***P < 0.001.

high density of postsynaptic receptors opposite the input axonal terminals. This allows for an efficient propagation of GABA mediated signals, which mostly result in neuronal inhibition. A key organizer for $GABA_A$ receptors is gephyrin that forms oligomeric superstructures beneath the synaptic area[24,25]. In addition, gephyrin plays a crucial role in synaptic dynamics and is a platform for multiple protein-protein interactions and bringing receptors. Thus, we examined the distribution of gephyrin as an indicator for functional $GABA_A$ receptors in amygdala[26]. In *Lis1*$^{+/+}$ mice, somata and proximal dendrites of amygdala neurons exhibited a variety of gephyrin clusters from very small round puncta to large and bright clusters (Fig. 5b). While *Lis1*$^{+/-}$ mice displayed similar pattern of gephyrin clusters with *Lis1*$^{+/+}$ mice, they were significantly decreased (Fig. 5b, e). Decreased gephyrin clusters in *Lis1*$^{+/-}$ mice were rescued by SNJ1945 treatment commencing at P10 (Fig. 5b, e). Thus, we concluded that post-natal treatment of SNJ1945 was effective for recovery of defective network formation and decreased receptor distribution in amygdala.

SNJ1945 augmented retrograde transport of nerve growth factor (NGF) in dorsal root ganglia (DRG) neurons. Neural growth

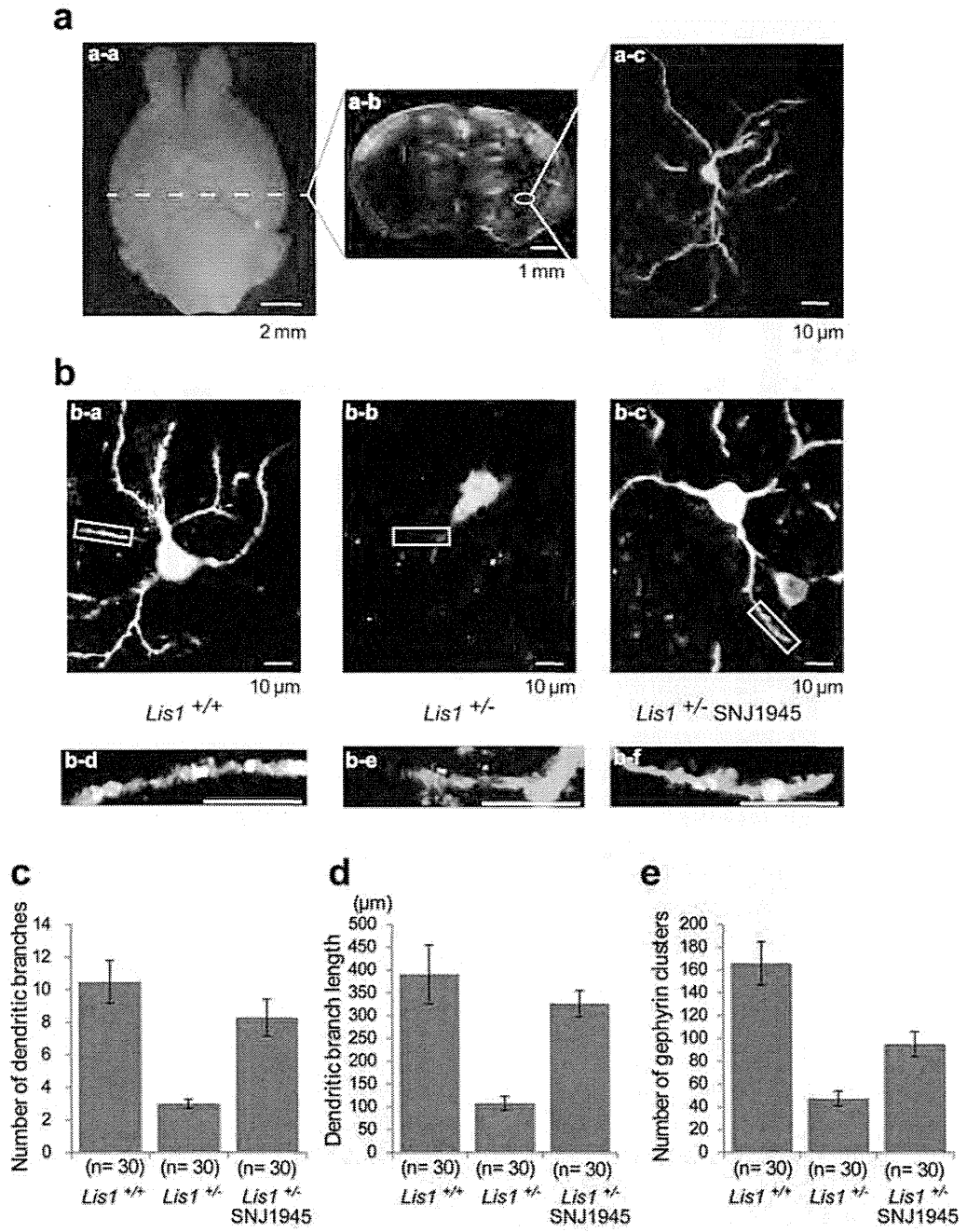

Figure 5 | Examination of neuronal networks and clustering of GABA receptors. (a) Neural fibers were visualized by the expression of TdTomato through *in utero* gene transfer. Ventral view image of whole brain by fluorescence dissecting microscope (a-a), confocal images at low (a-b) and high magnifications of representative fields (a-c) from coronal amygdala (white circle) are shown. (b) Individual image of amygdala neurons. Neural fiber was visualized by the TdTomato expression (red), which was decorated by gephyrin clusters (green). Representative images from *Lis1*$^{+/+}$ mice (b-a, d), *Lis1*$^{+/-}$ mice (b-b, e) and *Lis1*$^{+/-}$ mice with P10 treatment (b-c, f) are shown. Note: *Lis1*$^{+/-}$ mice exhibited poor arbors of neural fiber and decreased clusters of gephyrin, which were rescued by the treatment of SNJ1945. We examined five independent transfected brains for each, which were subjected to serial cryostat section with 5 μm thickness. Statistical examination of branching frequency (c), total length of branches (d) and number of gephyrin clusters (e) was performed.

factors are crucially important for activity-dependent plastic changes in synaptic strength and network refinement. We assumed that the SNJ1945 dependent rescue of neural network formation and receptor distribution might be attributable to the recovery of retrograde transport of neural growth factors. Retrograde axonal transport of nerve growth factor (NGF) signals is critical for the survival, differentiation, and maintenance of peripheral sympathetic and sensory neurons and basal forebrain cholinergic neurons. To examine retrograde transport of NGF, we used quantum dots (Qd-NGF) to track retrograde transport of NGF in cultures of mouse DRG neurons. Using pseudoTIRF microscopy, we tracked the movement of Qd-NGF in live DRG neurons in real time[27]. We applied non-compartmentalized cultures of DRG neurons, which displayed both directional movements of Qd-NGFs. Live-cell

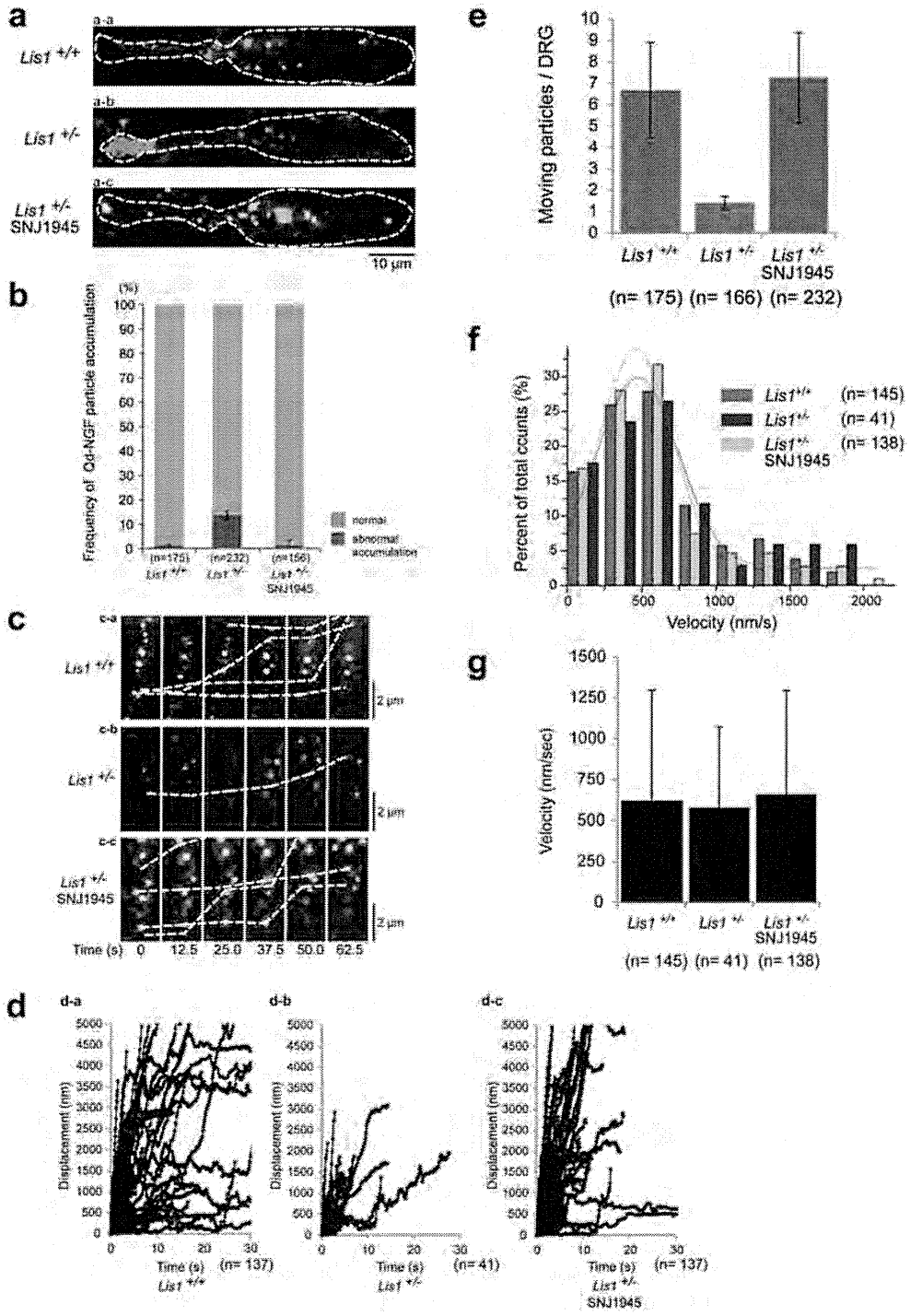

Figure 6 | Retrograde transport of NGF in DRG neurons. To show that the Qd-NGF complex can be internalized at axon terminals and transported in a retrograde fashion to neuron cell bodies, quantum dots were conjugated to NGF (Qd-NGF) and incubated with DRG neurons followed by pseudoTIRF microscope examination. (a) Qd-NGF were internalized and transported to the cell body. White dotted line indicates the contour of DRG neurons. DRG neurons from *Lis1*$^{+/+}$ mice (a-a), *Lis1*$^{+/-}$ mice (a-b) and *Lis1*$^{+/-}$ mice with P10 treatment (a-c) are shown. Note: in *Lis1*$^{+/-}$ mice, Qd-NGF dots were internalized, but aberrantly accumulated at the tips of DRG neurons (red arrowhead). (b) Each percentage of abnormal accumulation was presented as mean ± SEM. n indicates the number of examined DRG neurons. Aberrant accumulation was exclusively observed in in *Lis1*$^{+/-}$ mice, which was rescued by SNJ1945 treatment. (c) Transport dynamics of Qd-NGF containing endosomes. Time-lapse video images of endosomes are shown. Lapsed time is shown at the bottom of panel. Retrograde transport of Qd-NGF containing endosomes in *Lis1*$^{+/-}$ mice was decreased (c-b). (d) Trajectories of endosomes from *Lis1*$^{+/+}$ mice (d-a), *Lis1*$^{+/-}$ mice (d-b) and *Lis1*$^{+/-}$ mice with P10 treatment (d-c) are shown. (e) Number of transported endosomes per DRG neuron was presented as mean ± SEM. n indicates the number of examined DRG neurons. Note: We found that significant reduction of the frequency in *Lis1*$^{+/-}$ mice, which was rescued by SNJ1945 treatment. (f) Histograms of velocities of retrograde-directed endosomes. (g) Mean velocities are 0.62 μm/s in *Lis1*$^{+/+}$ mice, 0.60 μm/s in *Lis1*$^{+/-}$ mice and 0.65 μm/s in *Lis1*$^{+/-}$ mice with P10 treatment. There was no significant difference in each group.

imaging revealed that Qd-NGFs were internalized at axon terminals and transported in a retrograde fashion to cell bodies in DRG neurons from *Lis1*$^{+/+}$ mice (Supplementary movie 1). Importantly, Qd-NGFs were internalized, but accumulate aberrantly at tips of DRG neurons from *Lis1*$^{+/-}$ mice (Fig. 6a, b). This aberrant accumulation was rescued by treatment of SNJ1945 (Fig. 6a, b). Our observations were similar with transport defects peroxisomes and endosomes in the genetic absence of *Lis1/nudF* of filamentous fungus *Aspergillus nidulans*[28]. Next, we characterized the transport of Qd-NGF containing endosomes. Kymographs from time-lapse videos of Qd-NGFs indicated that the retrograde transport of Qd-NGF containing endosomes moved in a stop-and-go manner (Fig. 6c, d, Supplementary movie 1). Strikingly, we found that the frequency of retrograde transport of Qd-NGF containing endosomes was significantly decreased in DRG neurons from *Lis1*$^{+/-}$ mice (Fig. 6c, d, e, Supplementary movie 2), whereas the frequency of anterograde transport of Qd-NGF containing endosomes was not affected (Supplementary Fig. 9). In clear contrast, the velocity of retrograde transport of Qd-NGF containing endosomes was intact in DRG neurons from *Lis1*$^{+/-}$ mice (Fig. 6f, g), which was also consistent with *Aspergillus nidulans*[28]. We next examined the effect of SNJ1945 in the decreased frequency of the retrograde transport. Importantly, the treatment of SNJ1945 clearly recovered the defective retrograde transport of Qd-NGF containing endosomes (Fig. 6c, d, e, Supplementary movie 3). Presumably, the protection of LIS1 degradation by SNJ1945 restored proper dynein distribution, resulting in the recovery of retrograde transport of Qd-NGF containing endosomes, which may stimulate network formation and receptor distribution.

Discussion

SNJ1945 is permeable to the BBB, and was effective in rescuing defects in *Lis1*$^{+/-}$ mice after treatment commenced perinatally. These findings suggest that SNJ1945 may be considered for the treatment of lissencephaly patients postnatally. In support of this, we demonstrated that SNJ1945 improved behavioral performances and brain glucose metabolism after treatment ten days after birth without histological rescue of brain disorganization. We also demonstrated that SNJ1945 stimulated network formation and receptor distribution, explaining functional rescue by SNJ1945. These functional rescues are partially attributable to restoration of growth signal, characterized by the recovery of retrograde transport of Qd-NGF containing endosomes. These findings support a potential therapeutic approach with a novel calpain inhibitor, SNJ1945, in the human ILS patient that has a *LIS1* mutation.

Methods

BrdU birthdating and proliferation studies. All mouse experiments were performed under the approval from the experimental animal committee of Osaka City University Graduate School of Medicine or the approval of the experimental animal committee of Osaka City University Graduate School of Medicine, National Institute for Physiological Sciences and Fujita Health University.

For bromodeoxyuridine (BrdU) experiments, pregnant dams (E15.5) were injected with BrdU (50 μg/g, i.p.), and the distribution of BrdU-positive cells was determined at P5. For pulse labeling to examine proliferation of neuroepithelial stem cell, pregnant dams (E13.5) were injected with BrdU (150 μg/g, i.p.). Subsequently, the distribution of BrdU-positive cells was determined one hour after injection. The incorporation of BrdU in cells was detected with a mouse anti-BrdU monoclonal primary antibody (Roche) followed by an alkaline phosphatase-conjugated secondary antibody (Boehringer Mannheim). We analyzed three independent mice for each genotype.

Histological examination and immunohistochemistry. After perfusion with 4%PFA fixative, tissues from wild type and mutant mice were embedded in paraffin and sectioned at 5 μm thickness. After deparaffination, endogenous peroxidase activity was blocked by incubating the sections in 1.5% peroxide in methanol for 20 min. The sections were then boiled in 0.01 M/liter citrate buffer, pH 6.0, for 20 min and cooled slowly. Before staining, the sections were blocked with rodent block (LabVision) for 60 min. The sections were washed in PBS and incubated with an anti-Brn-1 antibody (Santa Cruz).

Cell culture and immunocytochemistry. Human fibroblasts were grown in D-MEM supplemented with 10% FBS. To inhibit calpain, cells were incubated with 200 μM SNJ1945 or control DMSO for 2 hrs. Cells were fixed in 4% PFA in PBS followed by permealization with 0.2% Triton X-100 in PBS. Coverslips were blocked for one hour with Block Ace (Yukijirushi) in PBS supplemented with 5% BSA, and were incubated for 1 hr in primary antibody, washed, and incubated for 1 hr using Alexa 546-conjugated secondary antibodies (Molecular Probes). Primary antibodies were an anti-βCOP antibody (Sigma) and an anti-DIC1 antibody (Chemicon).

Behavioral analysis. *Lis1*$^{+/+}$ mice and *Lis1*$^{+/-}$ mice that were treated with and without SNJ1945 were used for behavioral experiments, as described in the figure legend for Figure 2a. *Lis1*$^{+/-}$ mice had a single *Lis1* mutant allele. In this study mice were on an FVB background. All behavioral tests were carried out with male mice that were at least 9 weeks old at the start of testing. Raw data from the behavioral tests, the date on which each experiment was performed, and the age of the mice at the time of the experiment are shown in the mouse phenotype database (http://www.mouse-phenotype.org/). Mice were group-housed (four mice per cage) in a room with a 12 h light/dark cycle (lights on at 7:00 a.m.) with access to food and water *ad libitum*. The room temperature was kept at 23 ± 2°C. Behavioral testing was performed between 9:00 a.m. and 6:00 p.m. After the tests, all apparatus were cleaned with diluted sodium hypochlorite solution to prevent a bias due to olfactory cues. Three independent groups of mice were prepared for behavioral tests. One group consisted of equal numbers of mice. *Lis1*$^{+/+}$; *Lis1*$^{+/+}$ mice without treatment, *Lis1*$^{+/-}$; *Lis1*$^{+/-}$ mice without treatment, *Lis1*$^{+/-}$E9.5; *Lis1*$^{+/-}$ mice with oral administration from from E9.5 (200 μg/g) followed by oral administration after birth (200 μg/g), *Lis1*$^{+/-}$P0; *Lis1*$^{+/-}$ mice with oral administration from peri-natal period (200 μg/g) *Lis1*$^{+/-}$P10; *Lis1*$^{+/-}$ mice with oral administration from ten days after birth (200 μg/g). Experiments were done in the following sequences; the first group (12 each): the general health and neurological screen including wire hang test (GHNS), light/dark transition (LD), rotarod (RR) and gait analysis (GA); the second group (16 each): GHNS, LD, RR and GA; the third group (24 each): GHNS, LD, open field (OF), elevated plus maze (EP), hot plate (HP), one-chamber social interaction test (SI), RR, Crawley's sociability and preference for social novelty test (CSI), startle response/prepulse inhibition test (PPI), Porsolt forced swim test (PS), fear conditioning test (FZ), tail suspension test (TS), and social interaction test in home cage (HC-SI). Behavioral data were obtained automatically by applications based on the public domain Image J program and modified for each test by Tsuyoshi Miyakawa (available through O'HARA & CO., Tokyo, Japan)[29]. Each behavioral test was separated from each other at least by 1 day.

Briefly, the rotarod test, using an accelerating rotarod (UGO Basile Accelerating Rotarod), was performed by placing mice on rotating drums (3 cm diameter) and measuring the time each animal was able to maintain its balance on the rod. The speed of the rotarod accelerated from 4 to 40 rpm over a 5-min period. Gait analysis was performed using ventral plane videography as described. Mice were placed on the treadmill belt that moves at a speed of 24.7 cm/s. Digital video images of the underside of mice were collected at 150 frames per second. The paw area indicates the temporal placement of the paw relative to the treadmill belt. The color images were converted to their binary matrix equivalents, and the areas (in pixels) of the approaching or retreating paws relative to the belt and camera were calculated throughout each stride. Plotting the area of each digital paw print (paw contact area) imaged sequentially in time provides a dynamic gait signal, representing the temporal record of paw placement relative to the treadmill belt. For Porsolt forced swimming test, the apparatus consisted of four plastic cylinders (20 cm height × 10 cm diameter). The cylinders were filled with water (23°C) up to a height of 7.5 cm. Mice were placed into the cylinders, and their behavior recorded over a 10-min test period. Data acquisition and analysis were performed automatically, using Image PS software (see above). All behavioral testing procedures were approved by the Animal Care and Use Committee of National Institute for Physiological Sciences and Fujita Health University.

MicroPET scan and data analysis. PET imaging data were obtained in male mice (20–30 g) using a small animal PET camera (microPET Focus-220, Simens Medical Systems), which has a transaxial resolution of 1.4 mm in full width at half-maximum. Data were acquired in a 128 × 128 × 95 matrix with a pixel of 0.475 mm and a slice thickness of 0.796 mm. Before PET scanning, mice were intravenously injected with ^{18}F-FDG (approximately 0.5 MBq/g B.W.) through a cannula inserted into the tail vein and were kept in their home cage for 30 min for the ^{18}F-FDG uptake under freely moving condition. Subsequently, the mice were placed in the small-animal PET scanner under isoflurane anesthesia (4% for induction and 1.5% for maintenance) with O_2 and N_2O gas. Static acquisitions were performed during 30 min. PET images were reconstructed using a filtered backprojection (FBP) algorithm. The image data acquired from microPET were analyzed by ASIPro VM (ver. 6.0, Concorde Microsystems Inc.) and PMOD (ver. 3.4, PMOD Technologies Ltd.) software. The PET and magnetic resonance (MR) images were co-registered using a PMOD software. MR images were obtained from *Lis1*$^{+/+}$ mice and *Lis1*$^{+/-}$ mice used for the PET study under isoflurane anesthesia with a 7 tesla MR scanner (BioSpec 70/20, Bruker). Volumetric regions of interest were placed on the several brain regions (striatum, cerebral cortex, hippocampus, thalamus, cerebellum, hypothalamus, amygdala, basal forebrain and septum, brain stem, midbrain, superior colliculi) based on the MR images. Relative regional ^{18}F-FDG uptake was determined by normalized count data to those in the whole brain. Each value was presented as mean ± SEM. Statistical analysis was performed using the SPSS Statistics Student software. Data

were analyzed using one-way ANOVA followed by *post hoc* Tukey's test for comparison among groups. Significance threshold was assumed at $P < 0.05$.

***In utero* transfection.** Expression vectors were introduced into fetal brains by an *in utero* electroporation-mediated gene transfer method[20]. Briefly, pregnant mice were deeply anesthetized on E16.5, and the uterine horns were exposed. Approximately 2 μl of *TdTomato* plasmid solution was injected into the lateral ventricle from outside the uteri with a glass micropipette (GD-1.5, Narishige, Tokyo, Japan). Each embryo in the uterus was then placed between the tweezers-type electrodes described above and electronic pulses (45 V; 50 msec duration) were applied five times at intervals of 950 msec (GUY21, Bexco ltd). The uterine horns were then placed back into the abdominal cavity to allow the embryos to continue normal development. Histological examination was performed 5 days after *in utero* injection (P2-P3). Histological examination was performed 35 days after *in utero* injection (P30). SNJ1045 as applied from P10 by oral administration.

Examination of retrograde transport of NGF by pseudoTIRF microscope and live imaging. NGF was conjugated with Qd655 via carboxyl group substitution by using the coupling reagent 1-ethyl-3-(3-dimethylaminopropyl) -carbodiimide (EDAC) (Pierce Biotech, Rockford, IL). An inverted microscope (Olympus 1 × 71) was modified for pseudoTIRF illumination. The laser beam (488 nm) was focused at the back focal plane of the objective lens (ApoN×60, 1.49 Oil, Olympus). The incident angle was adjusted to be slightly smaller than the critical angle so that the laser beam could penetrate ≈1 μm into the aqueous solution. To image transport of Qd-NGF in live neurons, DRG neurons were incubated with Qd-NGF. Fluorescence images were filtered with a Qd655/15 emission filter. Time-lapse images were acquired by using an EMCCD camera (ImageM, Hamamatsu photonics) at the speed of 5–10 frames per second.

LC-MS/MS analysis. The SNJ1945 concentration in the brain was determined by turbo ion spray on an API 4000 triple-quadrupole mass spectrometer (Applied Biosystems) equipped with a turbo ion spray source using multiple reaction monitoring (MRM). Chromatography was performed on a NANOSPACE SI-2 HPLC system (Shiseido) with Shiseido Capcell pak C18 MG-II column. The extraction of SNJ1945 from the brain and the measuring condition were described in the literature[9].

1. Beckmann, N. *et al.* In vivo mouse imaging and spectroscopy in drug discovery. *NMR Biomed* **20**, 154–185 (2007).
2. Reiner, O. *et al.* Isolation of a Miller-Dieker lissencephaly gene containing G protein beta-subunit-like repeats. *Nature* **364**, 717–721 (1993).
3. Hattori, M., Adachi, H., Tsujimoto, M., Arai, H. & Inoue, K. Miller-Dieker lissencephaly gene encodes a subunit of brain platelet-activating factor acetylhydrolase [corrected]. *Nature* **370**, 216–218 (1994).
4. Vallee, R. B., Tai, C. & Faulkner, N. E. LIS1: cellular function of a disease-causing gene. *Trends Cell Biol* **11**, 155–160 (2001).
5. Wynshaw-Boris, A. Lissencephaly and LIS1: insights into the molecular mechanisms of neuronal migration and development. *Clin Genet* **72**, 296–304 (2007).
6. Yamada, M. *et al.* LIS1 and NDEL1 coordinate the plus-end-directed transport of cytoplasmic dynein. *Embo J* **27**, 2471–2483 (2008).
7. Yamada, M. *et al.* Inhibition of calpain increases LIS1 expression and partially rescues in vivo phenotypes in a mouse model of lissencephaly. *Nat Med* **15**, 1202–1207 (2009).
8. Koumura, A. *et al.* A novel calpain inhibitor, ((1S)-1((((1S)-1-benzyl-3-cyclopropylamino-2,3-di-oxopropyl)amino)carbonyl)-3-methylbutyl) carbamic acid 5-methoxy-3-oxapentyl ester, protects neuronal cells from cerebral ischemia-induced damage in mice. *Neuroscience* **157**, 309–318 (2008).
9. Shirasaki, Y., Yamaguchi, M. & Miyashita, H. Retinal penetration of calpain inhibitors in rats after oral administration. *J Ocul Pharmacol Ther* **22**, 417–424 (2006).
10. Oka, T. *et al.* Amelioration of retinal degeneration and proteolysis in acute ocular hypertensive rats by calpain inhibitor ((1S)-1-((((1S)-1-benzyl-3-cyclopropylamino-2,3-di-oxopropyl)amino)carbony l)-3-methylbutyl)carbamic acid 5-methoxy-3-oxapentyl ester. *Neuroscience* **141**, 2139–2145 (2006).
11. Sasaki, S. *et al.* Complete loss of Ndel1 results in neuronal migration defects and early embryonic lethality. *Mol Cell Biol* **25**, 7812–7827 (2005).
12. Hirotsune, S. *et al.* Graded reduction of Pafah1b1 (Lis1) activity results in neuronal migration defects and early embryonic lethality. *Nat Genet* **19**, 333–339 (1998).
13. Yingling, J. *et al.* Neuroepithelial stem cell proliferation requires LIS1 for precise spindle orientation and symmetric division. *Cell* **132**, 474–486 (2008).
14. McEvilly, R. J., de Diaz, M. O., Schonemann, M. D., Hooshmand, F. & Rosenfeld, M. G. Transcriptional regulation of cortical neuron migration by POU domain factors. *Science* **295**, 1528–1532 (2002).
15. Manent, J. B., Wang, Y., Chang, Y., Paramasivam, M. & LoTurco, J. J. Dcx reexpression reduces subcortical band heterotopia and seizure threshold in an animal model of neuronal migration disorder. *Nat Med* **15**, 84–90 (2009).
16. Paylor, R. *et al.* Impaired learning and motor behavior in heterozygous Pafah1b1 (Lis1) mutant mice. *Learn Mem* **6**, 521–537 (1999).
17. Mizuma, H., Shukuri, M., Hayashi, T., Watanabe, Y. & Onoe, H. Establishment of in vivo brain imaging method in conscious mice. *J Nucl Med* **51**, 1068–1075 (2010).
18. Pfund, Z. *et al.* Lissencephaly: fetal pattern of glucose metabolism on positron emission tomography? *Neurology* **55**, 1683–1688 (2000).
19. Palmer, A. E. & Tsien, R. Y. Measuring calcium signaling using genetically targetable fluorescent indicators. *Nat Protoc* **1**, 1057–1065 (2006).
20. Takitoh, T. *et al.* Activation of Aurora-A Is Essential for Neuronal Migration via Modulation of Microtubule Organization. *J Neurosci* **32**, 11050–11066 (2012).
21. Davis, M., Walker, D. L. & Myers, K. M. Role of the amygdala in fear extinction measured with potentiated startle. *Ann N Y Acad Sci* **985**, 218–232 (2003).
22. LeDoux, J. E. Emotion circuits in the brain. *Annu Rev Neurosci* **23**, 155–184 (2000).
23. Pare, D., Quirk, G. J. & Ledoux, J. E. New vistas on amygdala networks in conditioned fear. *J Neurophysiol* **92**, 1–9 (2004).
24. Takahashi, H. *et al.* Selective control of inhibitory synapse development by Slitrk3-PTPdelta trans-synaptic interaction. *Nat Neurosci* **15**, 389–398, S381–382 (2012).
25. van Versendaal, D. *et al.* Elimination of inhibitory synapses is a major component of adult ocular dominance plasticity. *Neuron* **74**, 374–383 (2012).
26. Chhatwal, J. P., Myers, K. M., Ressler, K. J. & Davis, M. Regulation of gephyrin and GABAA receptor binding within the amygdala after fear acquisition and extinction. *J Neurosci* **25**, 502–506 (2005).
27. Cui, B. *et al.* One at a time, live tracking of NGF axonal transport using quantum dots. *Proc Natl Acad Sci U S A* **104**, 13666–13671 (2007).
28. Egan, M. J., Tan, K. & Reck-Peterson, S. L. Lis1 is an initiation factor for dynein-driven organelle transport. *J Cell Biol* **197**, 971–982 (2012).
29. Yamasaki, N. *et al.* Alpha-CaMKII deficiency causes immature dentate gyrus, a novel candidate endophenotype of psychiatric disorders. *Mol Brain* **1**, 6 (2008).

Acknowledgements

We thank Azusa Inagaki, Kaori Nakakubo, Yukimi Kira and Yoriko Yabunaka for technical support, Hiromichi Nishimura and Keiko Fujimoto for mouse breeding. This work was supported by Grant-in-Aid for Scientific Research from the Ministry of Education, Science, Sports and Culture of Japan from the Ministry of Education, Science, Sports and Culture of Japan to Shinji Hirotsune and Knowledge Cluster Initiative (Stage-2) Research Foundation to Shinji Hirotsune. This work was also supported by Takeda Science Foundation and the Sumitomo Foundation to Shinji Hirotsune and NIH grants NS41030 and HD47380 to Anthony Wynshaw-Boris. This work was also supported in part by Grant-in-Aid for Scientific Research(B) of Japan Society for the Promotion of Science (JSPS)(#22390056 to Masami Yamada), Adaptable and Seamless Technology Transfer Program (A-STEP) through Target-driven R&D, Japan Science and Technology Agency (#AS231Z02224G to Masami Yamada), Grant-in-Aid for Scientific Research on Innovative Areas of The Ministry of Education, Culture, Sports, Science and Technology (MEXT)(#11001981 to Masami Yamada) and The Uehara Memorial Foundation (to Masami Yamada). This work was also supported by KAKENHI (Grant-in-Aid for Scientific Research) on Young Scientists A (16680015), Scientific Research (B) (21300121, 21390069), Exploratory Research (19653081), Integrative Brain Research (IBR-shien), and Innovative Areas (Comprehensive Brain Science Network) from the Ministry of Education, Science, Sports and Culture of Japan (MEXT) of Japan, grant from Neuroinformatics Japan Center (NIJC), grants from CREST of Japan Science and Technology Agency (JST), and the Funding Program for Next Generation World-Leading Researchers (Next Program). This work was also supported by the Multidisciplinary program for elucidating the brain development from molecules to social behavior (Fukui Brain Project) and the Grants-in-Aid for Scientific Research and Strategic Research Program for Brain Sciences ("integrated research on neuropsychiatric disorder") by the Ministry of Education, Culture, Sports, Science and Technology of Japan to Makoto Sato. We declare no conflicts of interests.

Author contributions

S.H. performed mouse histological examination and mouse behavioral analyasis. M.Y. performed mouse histological examination. K.T., S.H. and T.M. performed mouse behavioral analyasis (Figure 3). Y.K. and Y.T. performed PET analysis (Figure 4). K.K., Y.O., H.W. and M.S. performed neural circuit characterization (Figure 5, 6). M.A. provided us SNJ1945. K.H., M.A., K.T. and M.K. provided us a fibroblast cell line from the human lissencephaly patient. A.W.-B. and S.H. organized experiments and wrote a manuscript.

Additional information

Supplementary information accompanies this paper at http://www.nature.com/scientificreports

Competing financial interests: The authors declare no competing financial interests.

How to cite this article: Toba, S. *et al.* Post-natal treatment by a blood-brain-barrier permeable calpain inhibitor, SNJ1945 rescued defective function in lissencephaly. *Sci. Rep.* **3**, 1224; DOI:10.1038/srep01224 (2013).

Epilepsia, 54(7):1262–1269, 2013
doi: 10.1111/epi.12203

FULL-LENGTH ORIGINAL RESEARCH

Targeted capture and sequencing for detection of mutations causing early onset epileptic encephalopathy

*Hirofumi Kodera, †Mitsuhiro Kato, ‡[1]Alex S. Nord, ‡Tom Walsh, ‡Ming Lee, §Gaku Yamanaka, ¶Jun Tohyama, *†Kazuyuki Nakamura, #Eiji Nakagawa, **Tae Ikeda, ††Bruria Ben-Zeev, ‡‡Dorit Lev, ‡‡Tally Lerman-Sagie, §§Rachel Straussberg, ¶¶Saori Tanabe, ##Kazutoshi Ueda, ***Masano Amamoto, †††Sayaka Ohta, ‡‡‡Yutaka Nonoda, *Kiyomi Nishiyama, *Yoshinori Tsurusaki, *Mitsuko Nakashima, *Noriko Miyake, †Kiyoshi Hayasaka, ‡Mary-Claire King, *Naomichi Matsumoto, and *Hirotomo Saitsu

*Department of Human Genetics, Yokohama City University Graduate School of Medicine, Yokohama, Japan; †Department of Pediatrics, Yamagata University Faculty of Medicine, Yamagata, Japan; ‡Department of Genome Sciences and Department of Medicine, University of Washington, Seattle, Washington, U.S.A.; §Department of Pediatrics, Tokyo Medical University, Tokyo, Japan; ¶Department of Pediatrics, Nishi-Niigata Chuo National Hospital, Niigata, Japan; #Department of Child Neurology, National Center of Neurology and Psychiatry, Tokyo, Japan; **Division of Pediatric Neurology, Osaka Medical Center and Research Institute for Maternal and Child Health, Osaka, Japan; ††The Edmond and Lily Safra Children's Hospital, Sheba Medical Center, Ramat Gan, Israel; ‡‡Metabolic Neurogenetic Clinic, Wolfson Medical Center, Holon, Israel; §§Department of Neurogenetics, Schneider's Children Medical Center, Petah Tiqwa, Israel; ¶¶Department of Pediatrics, Nihonkai General Hospital, Sakata, Japan; ##Department of Pediatrics, Kitano Hospital, Osaka, Japan; ***Pediatric Emergency Center, Kitakyusyu City Yahata Hospital, Kitakyushu, Japan; †††Department of Pediatrics, Graduate School of Medicine, University of Tokyo, Tokyo, Japan; and ‡‡‡Department of Pediatrics, School of Medicine, Kitasato University, Sagamihara, Japan

Summary

Purpose: Early onset epileptic encephalopathies (EOEEs) are heterogeneous epileptic disorders caused by various abnormalities in causative genes including point mutations and copy number variations (CNVs). In this study, we performed targeted capture and sequencing of a subset of genes to detect point mutations and CNVs simultaneously.

Methods: We designed complementary RNA oligonucleotide probes against the coding exons of 35 known and potential candidate genes. We tested 68 unrelated patients, including 15 patients with previously detected mutations as positive controls. In addition to mutation detection by the Genome Analysis Toolkit, CNVs were detected by the relative depth of coverage ratio. All detected events were confirmed by Sanger sequencing or genomic microarray analysis.

Key Findings: We detected all positive control mutations. In addition, in 53 patients with EOEEs, we detected 12 pathogenic mutations, including 9 point mutations (2 nonsense, 3 splice-site, and 4 missense mutations), 2 frameshift mutations, and one 3.7-Mb microdeletion. Ten of the 12 mutations occurred de novo; the other two had been previously reported as pathogenic. The entire process of targeted capture, sequencing, and analysis required 1 week for the testing of up to 24 patients.

Significance: Targeted capture and sequencing enables the identification of mutations of all classes causing EOEEs, highlighting its usefulness for rapid and comprehensive genetic testing.

KEY WORDS: Target capture, Sequencing, Mutation, Copy number variation, Genetic testing.

Early onset epileptic encephalopathies (EOEEs), occurring before 1 year of age, are characterized by impairment of cognitive, sensory, and motor development by recurrent clinical seizures or prominent interictal epileptiform discharges (Berg et al., 2010). Ohtahara syndrome (OS), West syndrome (WS), early myoclonic encephalopathy (EME), migrating partial seizures in infancy (MPSI), and Dravet syndrome (DS) are the best known epileptic encephalopathies recognized by the International League Against Epilepsy (ILAE; Berg et al., 2010). However, many infants with similar features do not strictly fit the parameters of these syndromes.

To date, 11 genes have been shown to be associated with EOEEs (Mastrangelo & Leuzzi, 2012). The identification of

Accepted March 21, 2013; Early View publication May 10, 2013.
Address correspondence to Hirotomo Saitsu, Department of Human Genetics, Yokohama City University Graduate School of Medicine, 3-9 Fukuura, Kanazawa-ku, Yokohama 236-0004, Japan. E-mail: hsaitsu@yokohama-cu.ac.jp
[1]Present address: Genomics Division, Lawrence Berkeley National Laboratory, Berkeley, California, U.S.A.

causative mutations associated with EOEEs and their related phenotypes is useful for genetic counseling, and possibly for management of the patients; however, it is time-consuming and arduous to screen all known disease-causing genes one by one using Sanger sequencing or high-resolution melting curve analysis (Wittwer, 2009). In addition, copy number variations (CNVs) involving causative genes can also cause EOEEs (Saitsu et al., 2008; Mei et al., 2010; Saitsu et al., 2011, 2012b). Array comparative genomic hybridization (CGH) and multiplex ligation-dependent probe amplification (MLPA) are well established for the detection of CNVs; however, it is often difficult for array CGH to detect small CNVs such as a single-exon deletion and for MLPA to screen multiple genes at a time (Schouten et al., 2002; Dibbens et al., 2011; Mefford et al., 2011; Stuppia et al., 2012). Therefore, an integrated method that detects both point mutations and CNVs for multiple genes would be useful for comprehensive genetic testing in EOEEs.

Recent progress in massively parallel DNA sequencing in combination with target capturing has facilitated rapid mutation detection (Ng et al., 2009). It has been reported that CNVs involving disease-causing genes in patients with breast or ovarian cancer can be detected by target capture sequencing using the relative depth of coverage ratio (Walsh et al., 2010, 2011; Nord et al., 2011). Targeted capture and sequencing of patients with epileptic disorders has successfully identified potential disease-causing mutations in 16 of 33 patients (Lemke et al., 2012), revealing its efficacy for detecting mutations. However, the detection of both point mutations and CNVs has not been reported in patients with epilepsy.

In this study, we performed targeted capture and sequencing of a subset of 35 genes to detect mutations and CNVs simultaneously in 68 patients with EOEEs. By analyzing the relative depth of coverage ratio, we were able to detect microdeletions, in which the numbers of deleted exons varied from a single exon to all exons of two genes. In combination with rapid sequencing using a benchtop next-generation sequencer, our method provides a fast, comprehensive, and cost-effective method for genetic testing of patients with EOEE.

Methods

Patients

We examined 68 patients (36 male and 32 female) with EOEEs (20 patients with OS, 20 with WS, 3 with EME, 4 with MPSI, 2 with DS, and 19 with unclassified epileptic encephalopathy). Diagnoses were based on clinical features and characteristic patterns on electroencephalography. In 15 of 68 patients (10 male and five female), disease-causing mutations or CNVs had been previously identified in our laboratory, so these mutations were used as positive controls (Table 1) (Saitsu et al., 2008, 2010a,b, 2011, 2012b,c; Nonoda et al., 2013). Genomic DNA was isolated from blood leukocytes according to standard methods. Experimental protocols were approved by the Yokohama City University School of Medicine Institutional Review Board for Ethical Issues. Written informed consent for genetic testing was obtained from the guardians of all tested individuals prior to analysis.

Target capture sequencing and variant detection

A custom-made SureSelect oligonucleotide probe library (Agilent Technologies, Santa Clara, CA, U.S.A.) was designed to capture the coding exons of 35 genes; 5 of them were potential candidates for EOEEs based on unpublished data (for a list of the 30 of 35 genes, see Table 2). We designed 120-bp capture probes with 3× centered probe-tiling, and avoiding 20-bp overlap to repeat region using the Agilent e-Array Web-based design tool. To cover regions

Table 1. Known mutations and copy number variants used as positive controls

	Case	Sex	Chr	Genes	Reported mutations or copy number variants (positive controls)	Type	Deletion size (kb)	Refs
SNVs	27	F	9	*STXBP1*	c.1328T>G (p.Met443Arg)	Missense		Saitsu et al. (2008)
	69	M	X	*CASK*	c.1A>G	Missense		Saitsu et al. (2012b)
	241	M	X	*CDKL5*	c.145G>A (p.Glu49Lys)	Missense		–
Indels	95	M	9	*STXBP1*	c.388_389del (p.Leu130AspfsX11)	Deletion		Saitsu et al. (2010a)
	313	M	X	*CASK*	c.227_228del (p.Glu76ValfsX6)	Deletion		–
	26	F	9	*SPTAN1*	c.6619_6621del (p.Glu2207del)	Deletion		Saitsu et al. (2010b)
	220	M	9	*STXBP1*	c.1381_1390del (p.Lys461GlyfsX82)	Deletion		–
	16	M	9	*SPTAN1*	c.6923_6928dup (p.Arg2308_Met2309dup)	Duplication		Saitsu et al. (2010b)
	309	M	9	*SPTAN1*	c.6908_6916dup (p.Asp2303_Leu2305dup)	Duplication		Nonoda et al. (2013)
CNVs	12	F	9	*STXBP1, SPTAN1*	Del(9)(q33.33–q34.11)	Microdeletion	2150	Saitsu et al. (2008)
	22	M	9	*STXBP1*	*STXBP1* Ex4 deletion	Microdeletion	4.6	Saitsu et al. (2011)
	83	M	X	*CASK*	*CASK* Ex2 deletion	Microdeletion	111	Saitsu et al. (2012b)
	102	F	X	*MECP2*	Del(X)(q28)	Microdeletion		–
	204	M	9	*STXBP1, SPTAN1*	Del(9)(q33.33–q34.11)	Microdeletion	2850	Saitsu et al. (2011)
	214	F	X	*CDKL5*	Del(X)(q22.13)	Microdeletion	137	Saitsu et al. (2011)

SNVs, single nucleotide variants; Indels, insertion/deletions; CNVs, copy number variations.

Table 2. Sequence performance for 30 target genes

Gene	Cytoband	No. of coding exons	Mean read depth	%bases above 5× depth (%)	%bases above 10× depth (%)
ARHGEF9	Xq11.1–q11.2	10	206	100	100
ARX	Xp21.3	5	44	59.4–94.4	38.7–90.6
CASK	Xp11.4	27	201	95.9–100	95.9–100
CDKL5	Xp22.13	20	238	100	100
COL4A1	13q34	52	287	98.3–100	98.3–100
COL4A2	13q34	47	190	100	99.1–100
FOXG1	14q12	1	231	86.5–100	81.1–96.4
GABRG2	5q34	11	300	92.3	92.3
GRIN2A	16p13.2	13	310	100	100
KCNQ2	20q13.33	17	135	100	97.7–100
MAGI2	7q21.11	22	255	96–98.3	94.5–97.5
MAPK10	4q21.3	12	304	100	100
MECP2	Xq28	3	217	96.2	96.2
MEF2C	5q14.3	10	270	100	100
NTNG1	1p13.3	9	298	100	100
PCDH19	Xq22.1	6	212	100	100
PLCB1	20p12.3	32	293	100	100
PNKP	19q13.33	17	208	100	98.5–100
PNPO	17q21.32	7	210	100	100
SCN1A	2q24.3	26	345	100	100
SCN2A	2q24.3	26	323	100	100
SLC25A22	11p15.5	9	121	100	100
SLC2A1	1p34.2	10	209	100	98.8–100
SNPH	20p13	4	179	100	100
SPTAN1	9q34.11	56	277	100	100
SRGAP2	1q32.1	20	320	96.6	96.6
ST3GAL5	2p11.2	8	302	93.6–100	93.6–99.9
STXBP1	9q34.11	20	306	100	100
SYN1	Xp11.23	13	131	93.4–100	81–100
SYP	Xp11.23	6	146	100	99.1–100

where we could not design probes with the above settings, some probes from the SureSelect Human All Exon 50-Mb kit (Agilent Technologies) were added to the probe libraries. A total of 2,738 probes, covering 156 kb, were prepared. Exon capture, enrichment, and indexing were performed according to the manufacturer's instructions. Twenty-four captured libraries were mixed and sequenced on an Illumina MiSeq (Illumina, San Diego, CA, U.S.A.) with 150-bp paired-end reads. Image analysis and base calling were performed using the Illumina Real Time Analysis Pipeline version 1.13 and CASAVA software v.1.8 (Illumina) with default parameters. Sequence reads were aligned to the reference human genome (GRCh37: Genome Reference Consortium human build 37) with Novoalign (Novocraft Technologies, Selangor, Malaysia). After conversion of the SAM file to a BAM file with SAMtools (Li et al., 2009), duplicate reads were marked using Picard (http://picard.sourceforge.net/) and excluded from downstream analysis. Local realignment around insertion/deletions (indels) and base quality score recalibration were performed using the Genome Analysis Toolkit (DePristo et al., 2011). Single-nucleotide variants (SNVs) and indels were identified using the Genome Analysis Toolkit UnifiedGenotyper and filtered according to the Broad Institute's best-practice guidelines v.3 except for HaplotypeScore filtering. We excluded variants found in 147 exomes from healthy individuals previously sequenced in our laboratory. Variants were annotated using ANNOVAR (Wang et al., 2010). Candidate disease-causing mutations were confirmed by Sanger sequencing on a 3500xL Genetic Analyzer (Applied Biosystems, Foster City, CA, U.S.A.). The Human Gene Mutation Database professional 2012.3 (BIOBASE GmbH, Wolfenbuettel, Germany) was used to check whether the variants had been previously reported.

Copy number analysis using target capture sequence data

Copy number changes were analyzed based on the relative depth of coverage ratios (Nord et al., 2011). Raw coverage on the target regions was calculated by SAMtools using BAM files, in which duplicate reads were excluded. Raw coverage was normalized and corrected for GC content and bait capture bias. Next, the ratios were calculated by comparing the sample-corrected coverage to the median-corrected coverage for the other 23 samples. A sliding window (20 bp) was used to identify CNVs for which the majority of bases had a ratio ≤ 0.6 (loss) or ≥ 1.4 (gain). We visually inspected the ratio

data and judged whether the call was true or likely to be a false positive. A flow chart of our variant detection and copy number analysis scheme is illustrated in Fig. S1.

Genomic microarray analysis and cloning of deletion breakpoints

The microdeletion involving *SCN1A* and *SCN2A* was confirmed using a CytoScan HD Array (Affymetrix, Santa Clara, CA, U.S.A.) according to the manufacturer's protocol. Copy number alterations were analyzed using the Chromosome Analysis Suite (ChAS; Affymetrix) with NA32 (hg19) annotations. The junction fragment spanning the deletion was amplified by long polymerase chain reaction (PCR) using several primer sets based on putative breakpoints according to the microarray data. Long PCR was performed in a 20-μl volume, containing 30 ng genomic DNA, 1× buffer for KOD FX, 0.4 mM each dNTP, 0.3 μM each primer, and 0.3 U KOD FX polymerase (Toyobo, Osaka, Japan). The deletion junction fragments were obtained using the following primers: #409-F (5′-TCCACAGTTTACAAACATCTTTTCATGG-3′) and #409-R (5′-AGAAATTGGCTTGGTCAGTACCAGCA-3′) (1.6-kb amplicon). PCR products were electrophoresed on agarose gels stained with ethidium bromide, purified with ExoSAP (USB Technologies, Cleveland, OH, U.S.A.), and sequenced with BIGDYE TERMINATOR CHEMISTRY v.3 according to the manufacturer's protocol (Applied Biosystems).

Results

Target capture sequencing yielded an average of 26 Mb per sample (range 17–41 Mb per sample) on the target regions, resulting in an average read depth of 255 (range across all samples: 173–437). The coverage of the protein-coding sequences of the 30 target genes is shown in Table 2. Overall, 98.6% of targeted coding sequence bases were covered by 10 reads or more; however, some genes such as *ARX* and *FOXG1* were less well covered because of embedded repeat sequences (Fig. S2). To validate the performance of target capture sequencing for detecting mutations and CNVs, we analyzed 15 samples in which disease-causing mutations or microdeletions had been identified previously in our laboratory (Saitsu et al., 2008, 2010a,b, 2011, 2012b; Nonoda et al., 2013). All nine control point mutations and six control microdeletions were detected (Table 1; Fig. 1). These data indicate that our target capture sequencing method was able to detect both point mutations and microdeletions, including deletion of a single exon.

Examination of 53 previously unresolved EOEE patients by targeted capture and sequencing revealed mutations in 12 patients (Table 3). Every patient harbored a different

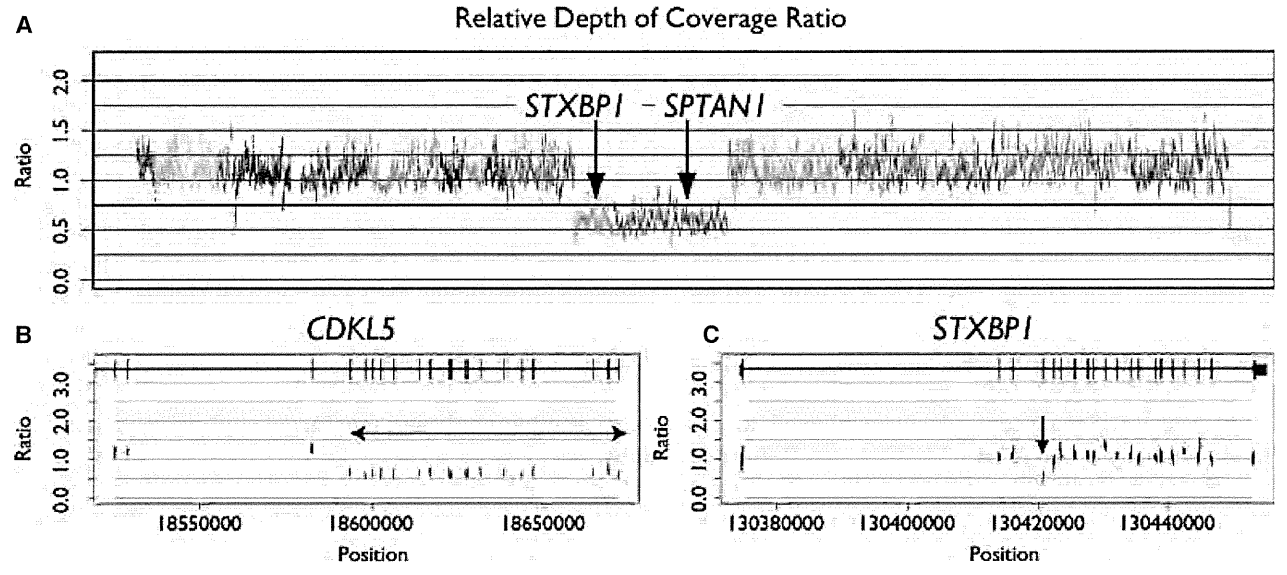

Figure 1.
Detection of three known microdeletions by target capture sequencing. (**A**) Relative depth of coverage ratio for patient 12. Coverage ratios for each target gene are indicated by different colors. A microdeletion including *STXBP1* and *SPTAN1* is clearly observed. (**B**, **C**) Relative depth of coverage ratio for patient 214 in the *CDKL5* region and patient 22 in the *STXBP1* region, respectively. Black vertical lines indicate exons and horizontal lines indicate introns (top). Red vertical lines show bait regions that were judged to be "deleted." A number of exons of *CDKL5* were deleted in patient 214 (bidirectional arrow in **B**), and a single exon of *STXBP1* was deleted in patient 22 (arrow in **C**).

Table 3. Mutations in 53 patients with EOEEs detected by targeted capture and sequencing

	Case	Sex	Diagnosis	Chr	Gene	Mutation	Type	Deletion size (kb)	Inheritance	References
SNVs	329	M	OS/EME	9	*STXBP1*	c.247-2A>G	Splice site		De novo	–
	402	M	OS	9	*STXBP1*	c.902+1G>A	Splice site		De novo	Milh et al. (2011)
	423	F	OS	9	*STXBP1*	c.246+1G>A	Splice site		De novo	–
	403	F	MAE or DS	2	*SCN1A*	c.580G>A (p.Asp194Asn)	Missense		Not found in the mother	Mancardi et al. (2006)
	415	F	EOEE	2	*SCN1A*	c.3714A>C (p.Glu1238Asp)	Missense		Not determined	Harkin et al. (2007)
	416	M	EOEE	X	*CDKL5*	c.533G>A (p.Arg178Gln)	Missense		De novo	Liang et al. (2011)
	418	F	WS, severe hypotonia	2	*SCN2A*	c.632G>A (p.Gly211Asp) in NM_001040143 (variant 3)	Missense		De novo	–
	244	F	Epilepsy + PCH	X	*CASK*	c.55G>T (p.Gly19X)	Nonsense		De novo	–
	404	F	EOEEs	X	*MECP2*	c.844C>T (p.Arg282X)	Nonsense		De novo	–
Indels	336	F	OS	9	*STXBP1*	c.1056del (p.Asp353ThrfsX3)	Deletion		De novo	–
	397	F	DS	2	*SCN1A*	c.342_344delinsAGGAGTT (p.Phe114LeufsX6)	Deletion–insertion		De novo	–
CNV	409	F	MPSI	2	*SCN2A*, *SCN1A*	Microdeletion	Microdeletion	3,726	De novo	–

OS, Ohtahara syndrome; EME, early myoclonic encephalopathy; MAE, myoclonic astatic epilepsy; DS, Dravet syndrome; WS, West syndrome; PCH, pontocerebellar hypoplasia; MPSI, malignant migrating partial seizures in infancy; SNVs, single nucleotide variants; CNVs, copy number variations; EOEEs, early onset epileptic encephalopathies.

mutation. Of these 12 mutations, 9 were single-nucleotide variants (2 nonsense, 3 splice-site, and 4 missense mutations) and two were small indels leading to frameshifts. The other mutation was a microdeletion. All these 11 point mutations were confirmed by Sanger sequencing. Four of the mutations (*STXBP1* c.902+1G>A, *SCN1A* c.580G>A, *SCN1A* c.3714A>C, and *CDKL5* c.533G>A) have been reported in individuals with EOEEs, so are recurrent (Mancardi et al., 2006; Harkin et al., 2007; Azmanov et al., 2010; Liang et al., 2011; Milh et al., 2011). Nine of the 11 mutations occurred de novo. The other two could not be tested because the paternal sample for one patient (*SCN1A* c.580G>A) and parental samples for another patient (*SCN1A* c.3714A>C) were unavailable.

CNV analysis of the 53 patients revealed a microdeletion involving *SCN1A* and *SCN2A* at 2q24.3 in patient 409 (Fig. 2A). To investigate this mutation further, we performed genomic microarray analysis and identified an approximately 3.7-Mb microdeletion (Fig. 2B). The deletion contained 13 RefSeq genes including *SCN2A* and *SCN1A*. Breakpoint-specific PCR analysis of the patient and her parents confirmed that the rearrangement occurred de novo (Fig. 2C). The sequence of the junction fragment confirmed a 3,726,029-bp deletion (chr2: 164,420,771–168,146,801) (Fig. 2D).

Discussion

Several bench-top high-throughput sequencing platforms are now available (Glenn, 2011; Loman et al., 2012; Quail et al., 2012). We selected Illumina MiSeq because it provides reasonable sequence throughput (1.6 Gb per run), a low error rate, a short run time (27 h), and sufficiently long reads (150 bp). We captured genomic DNA fragments of target genes by 3× tiling complementary RNA oligonucleotide probes (Nord et al., 2011) and sequenced 24 samples per MiSeq run, achieving sufficient coverage (a mean read depth of 255) over the target regions. This high coverage enabled us to detect point mutations and CNVs simultaneously, and long reads enabled us to detect small indels (Krawitz et al., 2010). Mapping by Novoalign, we were able to detect indels ranging in size from a 10-bp deletion to a 9-bp duplication.

By evaluating depth of coverage ratios (Nord et al., 2011), we detected six control microdeletions and one novel microdeletion, ranging in size from 4.6 kb to 3.7 Mb. To date, CNVs causing EOEEs have been analyzed by array CGH and MLPA (Mulley & Mefford, 2011). Array CGH can detect genome-wide CNVs, but its standard resolution is relatively low (>10 kb). On the other hand, MLPA can detect CNVs in specific genes, including single exon deletions; however, it is difficult to screen many genes at a time because MLPA is limited to 50 target exons per reaction (Stuppia et al., 2012). In addition, copy number analysis using MLPA can be affected by single nucleotide variants and indels in regions corresponding to the MLPA probes (Stuppia et al., 2012). In contrast, targeted capture and sequencing can analyze all targeted genes to detect mutations and CNVs simultaneously. CNVs as small as a single exon can be identified. Because all the procedures—from

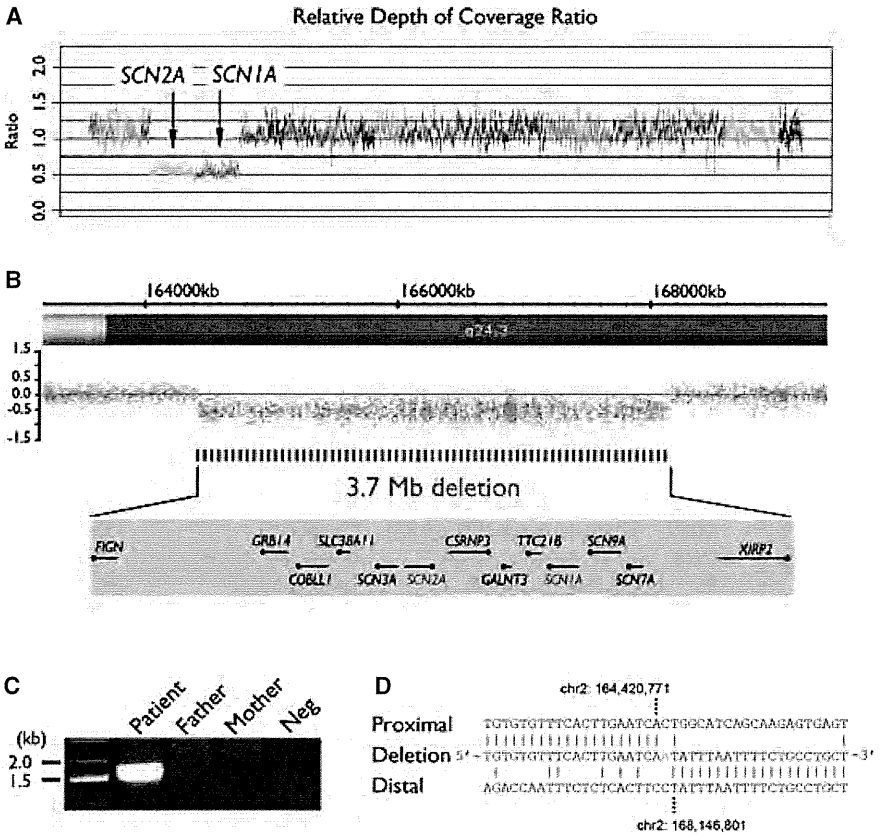

Figure 2.

A 3.7-Mb microdeletion including *SCN2A* and *SCN1A* in patient 409. (**A**) Relative depth of coverage ratio for patient 409 indicates a microdeletion encompassing *SCN2A* and *SCN1A*. Different colors distinguish the target genes. (**B**) The array profile clearly shows a 3.7-Mb microdeletion at 2q24.3 in this patient. Thirteen RefSeq genes, including *SCN2A* and *SCN1A*, lie within the microdeletion (bottom). (**C**) Breakpoint-specific PCR analysis of the patient's family. Primers flanking the deletion were able to amplify a 1,607-bp product from the patient only, indicating that the translocation occurred de novo. (**D**) Deletion junction sequence. The top, middle, and bottom strands show the proximal, deleted, and distal sequences, respectively. A single inserted nucleotide (colored in red) was identified at the breakpoint.

the capture of target genes to the detection of mutations and CNVs—can be done within a week, our workflow provides a fast, sensitive, and comprehensive genetic testing method for patients with epilepsy.

Whole-exome sequencing will reveal novel mutations in unexpected genes in patients with EOEEs. For example, *KCNQ2* mutations, which cause benign familial neonatal seizures (Biervert et al., 1998; Charlier et al., 1998), were identified in patients with OS by whole exome sequencing (Saitsu et al., 2012a). Similarly, screening known and potential candidate genes in patients with EOEEs will reveal novel mutations in unexpected genes, in addition to mutations in well-known genes.

In our target capture analysis, some exons of genes such as *ARX* and *FOXG1* were insufficiently sequenced because repeat sequences hampered the design of capture probes. Repeat sequences also interfere with appropriate mapping of sequence reads, resulting in low coverage. For these exons, Sanger sequencing should be added for complete analysis.

In conclusion, a rapid and efficient system of target capture sequencing can be applied to the comprehensive genetic analysis of EOEEs. Point mutations, small indels, and CNVs are all detected by this method, confirming the potential of this approach for efficient genetic testing.

Acknowledgments

We thank the patients and their families for their participation in this study. We also thank Aya Narita and Nobuko Watanabe for their technical assistance. This work was Supported by the Ministry of Health, Labour and Welfare of Japan (24133701, 11103577, 11103580, 11103340, 10103235), a Grant-in-Aid for Scientific Research (C) from the Japan Society for the Promotion of Science (24591500), a Grant-in-Aid for Young Scientists from the Japan Society for the Promotion of Science (10013428, 11001011, 12020465), the Takeda Science Foundation, the Japan Science and Technology Agency, the Strategic Research

Program for Brain Sciences (11105137), and a Grant-in-Aid for Scientific Research on Innovative Areas (Transcription Cycle) from the Ministry of Education, Culture, Sports, Science and Technology of Japan (12024421).

Disclosure

None of the authors has any conflicts of interest to disclose. We confirm that we have read the Journal's position on issues involved in ethical publication and affirm that this report is consistent with those guidelines.

References

Azmanov DN, Zhelyazkova S, Dimova PS, Radionova M, Bojinova V, Florez L, Smith SJ, Tournev I, Jablensky A, Mulley J, Scheffer I, Kalaydjieva L, Sander JW. (2010) Mosaicism of a missense SCN1A mutation and Dravet syndrome in a Roma/Gypsy family. *Epileptic Disord* 12:117–124.

Berg AT, Berkovic SF, Brodie MJ, Buchhalter J, Cross JH, van Emde Boas W, Engel J, French J, Glauser TA, Mathern GW, Moshe SL, Nordli D, Plouin P, Scheffer IE. (2010) Revised terminology and concepts for organization of seizures and epilepsies: report of the ILAE Commission on Classification and Terminology, 2005–2009. *Epilepsia* 51:676–685.

Biervert C, Schroeder BC, Kubisch C, Berkovic SF, Propping P, Jentsch TJ, Steinlein OK. (1998) A potassium channel mutation in neonatal human epilepsy. *Science* 279:403–406.

Charlier C, Singh NA, Ryan SG, Lewis TB, Reus BE, Leach RJ, Leppert M. (1998) A pore mutation in a novel KQT-like potassium channel gene in an idiopathic epilepsy family. *Nat Genet* 18:53–55.

DePristo MA, Banks E, Poplin R, Garimella KV, Maguire JR, Hartl C, Philippakis AA, del Angel G, Rivas MA, Hanna M, McKenna A, Fennell TJ, Kernytsky AM, Sivachenko AY, Cibulskis K, Gabriel SB, Altshuler D, Daly MJ. (2011) A framework for variation discovery and genotyping using next-generation DNA sequencing data. *Nat Genet* 43:491–498.

Dibbens LM, Kneen R, Bayly MA, Heron SE, Arsov T, Damiano JA, Desai T, Gibbs J, McKenzie F, Mulley JC, Ronan A, Scheffer IE. (2011) Recurrence risk of epilepsy and mental retardation in females due to parental mosaicism of PCDH19 mutations. *Neurology* 76: 1514–1519.

Glenn TC. (2011) Field guide to next-generation DNA sequencers. *Mol Ecol Resour* 11:759–769.

Harkin LA, McMahon JM, Iona X, Dibbens L, Pelekanos JT, Zuberi SM, Sadleir LG, Andermann E, Gill D, Farrell K, Connolly M, Stanley T, Harbord M, Andermann F, Wang J, Batish SD, Jones JG, Seltzer WK, Gardner A, Sutherland G, Berkovic SF, Mulley JC, Scheffer IE. (2007) The spectrum of SCN1A-related infantile epileptic encephalopathies. *Brain* 130:843–852.

Krawitz P, Rodelsperger C, Jager M, Jostins L, Bauer S, Robinson PN. (2010) Microindel detection in short-read sequence data. *Bioinformatics* 26:722–729.

Lemke JR, Riesch E, Scheurenbrand T, Schubach M, Wilhelm C, Steiner I, Hansen J, Courage C, Gallati S, Burki S, Strozzi S, Simonetti BG, Grunt S, Steinlin M, Alber M, Wolff M, Klopstock T, Prott EC, Lorenz R, Spaich C, Rona S, Lakshminarasimhan M, Kroll J, Dorn T, Kramer G, Synofzik M, Becker F, Weber YG, Lerche H, Bohm D, Biskup S. (2012) Targeted next generation sequencing as a diagnostic tool in epileptic disorders. *Epilepsia* 53:1387–1398.

Li H, Handsaker B, Wysoker A, Fennell T, Ruan J, Homer N, Marth G, Abecasis G, Durbin R. (2009) The sequence Alignment/Map format and SAMtools. *Bioinformatics* 25:2078–2079.

Liang JS, Shimojima K, Takayama R, Natsume J, Shichiji M, Hirasawa K, Imai K, Okanishi T, Mizuno S, Okumura A, Sugawara M, Ito T, Ikeda H, Takahashi Y, Oguni H, Imai K, Osawa M, Yamamoto T. (2011) *CDKL5* alterations lead to early epileptic encephalopathy in both genders. *Epilepsia* 52:1835–1842.

Loman NJ, Misra RV, Dallman TJ, Constantinidou C, Gharbia SE, Wain J, Pallen MJ. (2012) Performance comparison of benchtop high-throughput sequencing platforms. *Nat Biotechnol* 30:434–439.

Mancardi MM, Striano P, Gennaro E, Madia F, Paravidino R, Scapolan S, Dalla Bernardina B, Bertini E, Bianchi A, Capovilla G, Darra F, Elia M, Freri E, Gobbi G, Granata T, Guerrini R, Pantaleoni C, Parmeggiani A, Romeo A, Santucci M, Vecchi M, Veggiotti P, Vigevano F, Pistorio A, Gaggero R, Zara F. (2006) Familial occurrence of febrile seizures and epilepsy in severe myoclonic epilepsy of infancy (SMEI) patients with *SCN1A* mutations. *Epilepsia* 47:1629–1635.

Mastrangelo M, Leuzzi V. (2012) Genes of early-onset epileptic encephalopathies: from genotype to phenotype. *Pediatr Neurol* 46: 24–31.

Mefford HC, Yendle SC, Hsu C, Cook J, Geraghty E, McMahon JM, Eeg-Olofsson O, Sadleir LG, Gill D, Ben-Zeev B, Lerman-Sagie T, Mackay M, Freeman JL, Andermann E, Pelakanos JT, Andrews I, Wallace G, Eichler EE, Berkovic SF, Scheffer IE. (2011) Rare copy number variants are an important cause of epileptic encephalopathies. *Ann Neurol* 70:974–985.

Mei D, Marini C, Novara F, Bernardina BD, Granata T, Fontana E, Parrini E, Ferrari AR, Murgia A, Zuffardi O, Guerrini R. (2010) Xp22.3 genomic deletions involving the CDKL5 gene in girls with early onset epileptic encephalopathy. *Epilepsia* 51:647–654.

Milh M, Villeneuve N, Chouchane M, Kaminska A, Laroche C, Barthez MA, Gitiaux C, Bartoli C, Borges-Correia A, Cacciagli P, Mignon-Ravix C, Cuberos H, Chabrol B, Villard L. (2011) Epileptic and nonepileptic features in patients with early onset epileptic encephalopathy and *STXBP1* mutations. *Epilepsia.* 52:1828–1834.

Mulley JC, Mefford HC. (2011) Epilepsy and the new cytogenetics. *Epilepsia* 52:423–432.

Ng SB, Turner EH, Robertson PD, Flygare SD, Bigham AW, Lee C, Shaffer T, Wong M, Bhattacharjee A, Eichler EE, Bamshad M, Nickerson DA, Shendure J. (2009) Targeted capture and massively parallel sequencing of 12 human exomes. *Nature* 461:272–276.

Nonoda Y, Saito Y, Nagai S, Sasaki M, Iwasaki T, Matsumoto N, Ishii M, Saitsu H. (2013) Progressive diffuse brain atrophy in West syndrome with marked hypomyelination due to *SPTAN1* gene mutation. *Brain Dev* 35:280–283.

Nord AS, Lee M, King MC, Walsh T. (2011) Accurate and exact CNV identification from targeted high-throughput sequence data. *BMC Genomics* 12:184.

Quail MA, Smith M, Coupland P, Otto TD, Harris SR, Connor TR, Bertoni A, Swerdlow HP, Gu Y. (2012) A tale of three next generation sequencing platforms: comparison of Ion Torrent, Pacific Biosciences and Illumina MiSeq sequencers. *BMC Genomics* 13:341.

Saitsu H, Kato M, Mizuguchi T, Hamada K, Osaka H, Tohyama J, Uruno K, Kumada S, Nishiyama K, Nishimura A, Okada I, Yoshimura Y, Hirai S, Kumada T, Hayasaka K, Fukuda A, Ogata K, Matsumoto N. (2008) De novo mutations in the gene encoding STXBP1 (MUNC18-1) cause early infantile epileptic encephalopathy. *Nat Genet* 40:782–788.

Saitsu H, Kato M, Okada I, Orii KE, Higuchi T, Hoshino H, Kubota M, Arai H, Tagawa T, Kimura S, Sudo A, Miyama S, Takami Y, Watanabe T, Nishimura A, Nishiyama K, Miyake N, Wada T, Osaka H, Kondo N, Hayasaka K, Matsumoto N. (2010a) *STXBP1* mutations in early infantile epileptic encephalopathy with suppression-burst pattern. *Epilepsia* 51:2397–2405.

Saitsu H, Tohyama J, Kumada T, Egawa K, Hamada K, Okada I, Mizuguchi T, Osaka H, Miyata R, Furukawa T, Haginoya K, Hoshino H, Goto T, Hachiya Y, Yamagata T, Saitoh S, Nagai T, Nishiyama K, Nishimura A, Miyake N, Komada M, Hayashi K, Hirai S, Ogata K, Kato M, Fukuda A, Matsumoto N. (2010b) Dominant-negative mutations in alpha-II spectrin cause West syndrome with severe cerebral hypomyelination, spastic quadriplegia, and developmental delay. *Am J Hum Genet* 86:881–891.

Saitsu H, Kato M, Shimono M, Senju A, Tanabe S, Kimura T, Nishiyama K, Yoneda Y, Kondo Y, Tsurusaki Y, Doi H, Miyake N, Hayasaka K, Matsumoto N. (2011) Association of genomic deletions in the STXBP1 gene with Ohtahara syndrome. *Clin Genet* 81:399–402.

Saitsu H, Kato M, Koide A, Goto T, Fujita T, Nishiyama K, Tsurusaki Y, Doi H, Miyake N, Hayasaka K, Matsumoto N. (2012a) Whole exome sequencing identifies *KCNQ2* mutations in Ohtahara syndrome. *Ann Neurol* 72:298–300.

Saitsu H, Kato M, Osaka H, Moriyama N, Horita H, Nishiyama K, Yoneda Y, Kondo Y, Tsurusaki Y, Doi H, Miyake N, Hayasaka K, Matsumoto

N. (2012b) *CASK* aberrations in male patients with Ohtahara syndrome and cerebellar hypoplasia. *Epilepsia* 53:1441–1449.

Saitsu H, Osaka H, Nishiyama K, Tsurusaki Y, Doi H, Miyake N, Matsumoto N. (2012c) A girl with early-onset epileptic encephalopathy associated with microdeletion involving CDKL5. *Brain Dev* 34:364–367.

Schouten JP, McElgunn CJ, Waaijer R, Zwijnenburg D, Diepvens F, Pals G. (2002) Relative quantification of 40 nucleic acid sequences by multiplex ligation-dependent probe amplification. *Nucleic Acids Res* 30:e57.

Stuppia L, Antonucci I, Palka G, Gatta V. (2012) Use of the MLPA assay in the molecular diagnosis of gene copy number alterations in human genetic diseases. *Int J Mol Sci* 13:3245–3276.

Walsh T, Lee MK, Casadei S, Thornton AM, Stray SM, Pennil C, Nord AS, Mandell JB, Swisher EM, King MC. (2010) Detection of inherited mutations for breast and ovarian cancer using genomic capture and massively parallel sequencing. *Proc Natl Acad Sci USA* 107: 12629–12633.

Walsh T, Casadei S, Lee MK, Pennil CC, Nord AS, Thornton AM, Roeb W, Agnew KJ, Stray SM, Wickramanayake A, Norquist B, Pennington KP, Garcia RL, King MC, Swisher EM. (2011) Mutations in 12 genes for inherited ovarian, fallopian tube, and peritoneal carcinoma identified by massively parallel sequencing. *Proc Natl Acad Sci USA* 108:18032–18037.

Wang K, Li M, Hakonarson H. (2010) ANNOVAR: functional annotation of genetic variants from high-throughput sequencing data. *Nucleic Acids Res* 38:e164.

Wittwer CT. (2009) High-resolution DNA melting analysis: advancements and limitations. *Hum Mutat* 30:857–859.

Supporting Information

Additional Supporting Information may be found in the online version of this article:

Figure S1. Flow chart of our variant detection and copy number analysis scheme.

Figure S2. Insufficient coverage of reads in two genes rich in repetitive sequences.

ELSEVIER

Brain & Development xxx (2013) xxx–xxx

BRAIN & DEVELOPMENT
Official Journal of the Japanese Society of Child Neurology

www.elsevier.com/locate/braindev

Case report

Girl with a *PRRT2* mutation and infantile focal epilepsy with bilateral spikes

Hiroyuki Torisu [a,b,*], Kyoko Watanabe [c], Keiko Shimojima [d], Midori Sugawara [d], Masafumi Sanefuji [a], Yoshito Ishizaki [a], Yasunari Sakai [a], Hironori Yamashita [c], Toshiyuki Yamamoto [d], Toshiro Hara [a]

[a] *Department of Pediatrics, Graduate School of Medical Sciences, Kyushu University, Fukuoka, Japan*
[b] *Department of Pediatrics, Fukuoka Dental College Medical and Dental Hospital, Fukuoka, Japan*
[c] *Department of Pediatrics, Kokura Medical Center, Kitakyushu, Japan*
[d] *Tokyo Women's Medical University Institute for Integrated Medical Sciences, Tokyo, Japan*

Received 5 October 2012; received in revised form 18 May 2013; accepted 22 May 2013

Abstract

This paper documents the case of a female Japanese patient with infantile focal epilepsy, which was different from benign infantile seizures, and a family history of infantile convulsion and paroxysmal choreoathetosis. The patient developed partial seizures (e.g., psychomotor arrest) at age 14 months. At the time of onset, interictal electroencephalography (EEG) showed bilateral parietotemporal spikes, but the results of neurologic examination and brain magnetic resonance imaging were normal. Her seizures were well controlled with carbamazepine, and she had a normal developmental outcome. EEG abnormalities, however, persisted for more than 6 years, and the spikes moved transiently to the occipital area and began to resemble the rolandic spikes recognized in benign childhood epilepsy. Her father had paroxysmal kinesigenic dyskinesia, with an onset age of 6 years, and her youngest sister had typical benign infantile seizures. Genetic analysis demonstrated that all affected members had a heterozygous mutation of c.649_650insC in the proline-rich transmembrane protein-2 (*PRRT2*) gene. This case indicates that the phenotypic spectrum of infantile seizures or epilepsy with *PRRT2*-related pathology may be larger than previously expected, and that genetic investigation of the effect of *PRRT2* mutations on idiopathic seizures or epilepsy in childhood may help elucidate the pathological backgrounds of benign childhood epilepsy.

Keywords: Infantile focal epilepsy; Paroxysmal kinesigenic dyskinesia; Infantile convulsion and paroxysmal choreoathetosis (ICCA); PRRT2; Mutation; c.649_650insC

1. Introduction

Close observation and examination of patients with infantile seizures has established the existence of a clinically benign type of infantile seizure [1–3]. Further investigations discovered several subtypes of benign infantile seizures (BIS), including 4 genetically different types of benign familial infantile seizures (BFIS1-4), benign non-familial infantile seizures, benign infantile seizures associated with mild gastroenteritis, and benign infantile focal epilepsy with midline spikes and waves during sleep (BIMSE) [4]. In 2011–2012, mutations in the proline-rich transmembrane protein-2 (*PRRT2*) gene were found to be responsible for paroxysmal kinesigenic dyskinesia (PKD; OMIM: 128200), BFIS2, and infantile convulsion

* Corresponding author. Address: Department of Pediatrics, Graduate School of Medical Sciences, Kyushu University, Fukuoka 812-8582, Japan. Tel.: +81 92 642 5421; fax: +81 92 642 5435.
E-mail address: htorys@pediatr.med.kyushu-u.ac.jp (H. Torisu).

0387-7604/$ - see front matter © 2013 The Japanese Society of Child Neurology. Published by Elsevier B.V. All rights reserved.
http://dx.doi.org/10.1016/j.braindev.2013.05.009

Please cite this article in press as: Torisu H et al. Girl with a *PRRT2* mutation and infantile focal epilepsy with bilateral spikes. Brain Dev (2013), http://dx.doi.org/10.1016/j.braindev.2013.05.009

and paroxysmal choreoathetosis (ICCA; OMIM: 602066) [5–10]. Despite these advances in the identification of related genetic mutations, the entire clinical spectrum of *PRRT2*-related diseases has not been fully elucidated.

This report presents the case of a female Japanese patient with infantile focal epilepsy with parietotemporal spikes and a significant family history of ICCA. Her father and youngest sister had PKD and typical BIS, respectively (Fig. 1). All affected members had the *PRRT2* mutation c.649_650insC, frequently found in patients with BFIS2 and ICCA [6]. This case suggests underlying contribution of *PRRT2* to the development of paroxysmal diseases with stronger effects than previously expected.

2. Case report

The female patient (identified as II-1 in Fig. 1) was the first child of non-consanguineous Japanese parents. She was born via spontaneous vaginal delivery at 41 weeks gestation, without asphyxia. At birth, she weighed 2876 g and her head circumference was 33.0 cm. She developed normally, could control her head at 3 months, sit alone at 7 months, walk at 13 months, and speak a word at 12 months. At 14 months, she developed sudden-onset eye rolling and cyanosis that lasted for 1 min. This episode was thought to represent a seizure, and she had a similar episode 11 days later. Neurologic examination and brain magnetic resonance imaging results were normal. Interictal electroencephalography (EEG) during sleep revealed multifocal spikes in the bilateral centrotemporal areas (Fig. 2A). At 15 months, she developed sudden-onset staring associated with turning her head to the left, which progressed to a generalized tonic seizure that lasted for 3 min. Treatment with carbamazepine was initiated at that time. Seizures were well controlled by the medication, but the EEG abnormalities continued over 6 years and gradually changed to bilateral spikes similar to the rolandic spikes recognized in benign childhood epilepsy (Fig. 2B–D). At age 7 years and 10 months, the patient went off the medication and subsequently had a generalized seizure.

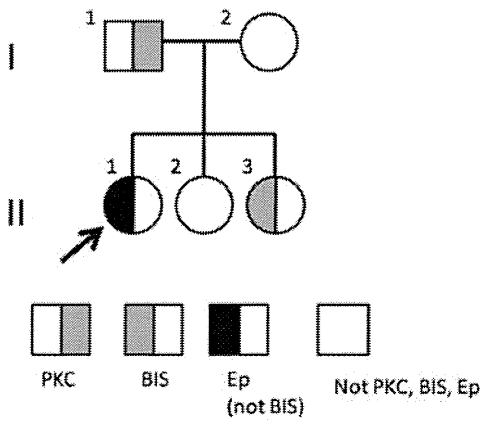

Fig. 1. Family pedigree. The proband (II-1) with epilepsy was the first child of I-1 with PKD. His third child (II-3) had BIS. PKD: paroxysmal kinesigenic dyskinesia, BIS: benign infantile seizure, Ep: epilepsy.

The father of the present patient (identified as I-1 in Fig. 1) had PKD. His dyskinetic movements began at age 6 years, but EEG at that time revealed no paroxysmal discharges. His development was normal with no developmental or neurologic problems and no febrile seizures since birth. His paroxysmal movements were well controlled with carbamazepine.

The youngest sister of the patient (identified as II-3 in Fig. 1) had 2 focal seizures at age 6 months. Again, her sister developed normally, without developmental or neurologic problems, and EEG did not show apparent epileptic discharges. After the focal seizures, carbamazepine therapy was initiated. She continued carbamazepine thereafter and continued to develop normally, with no further seizures.

After obtaining informed consent, the *PRRT2* gene was sequenced using DNA extracted from the peripheral blood of affected family members. A heterozygous frameshift mutation, c.649_650insC, was detected, resulting in p.Arg217Profs*8 (Fig. 3).

3. Discussion

The findings in this case indicate that epilepsy or seizures other than BIS could be associated with a *PRRT2* mutation. This association is supported by a few previous reports describing patients having a *PRRT2* mutation with epilepsy, including absence epilepsy [6,7]. The molecular function of the encoded protein PRRT2 has not been fully defined. PRRT2 is likely expressed in the brain and spinal cord in the embryonic and postnatal stages of development [5,6,8]. PRRT2 is thought to interact with a 25-kDa synaptosomal-associated protein (SNAP25) [8]. SNAP25 is a part of the soluble *N*-ethylmaleimide-sensitive factor attachment protein receptor (SNARE) proteins, which fuse synaptic vesicles to the presynaptic plasma membrane and release neurotransmitters. Defects in synaptic functions are predicted to be associated with brain disorders, including epilepsy, and PRRT2 dysfunction may disturb nerve conduction in the central nervous system and cause various types of paroxysmal diseases. The current case indicates that there may be a larger phenotypic spectrum of infantile seizures or epilepsy, with PRRT2-related molecular pathology, than previously expected. Future investigations should explore the involvement of PRRT2 in the pathology of paroxysmal disorders.

However, the current case may be a rare case with a *PRRT2* mutation incidentally occurring with other epileptic backgrounds. Despite considerable phenotypic

Please cite this article in press as: Torisu H et al. Girl with a *PRRT2* mutation and infantile focal epilepsy with bilateral spikes. Brain Dev (2013), http://dx.doi.org/10.1016/j.braindev.2013.05.009

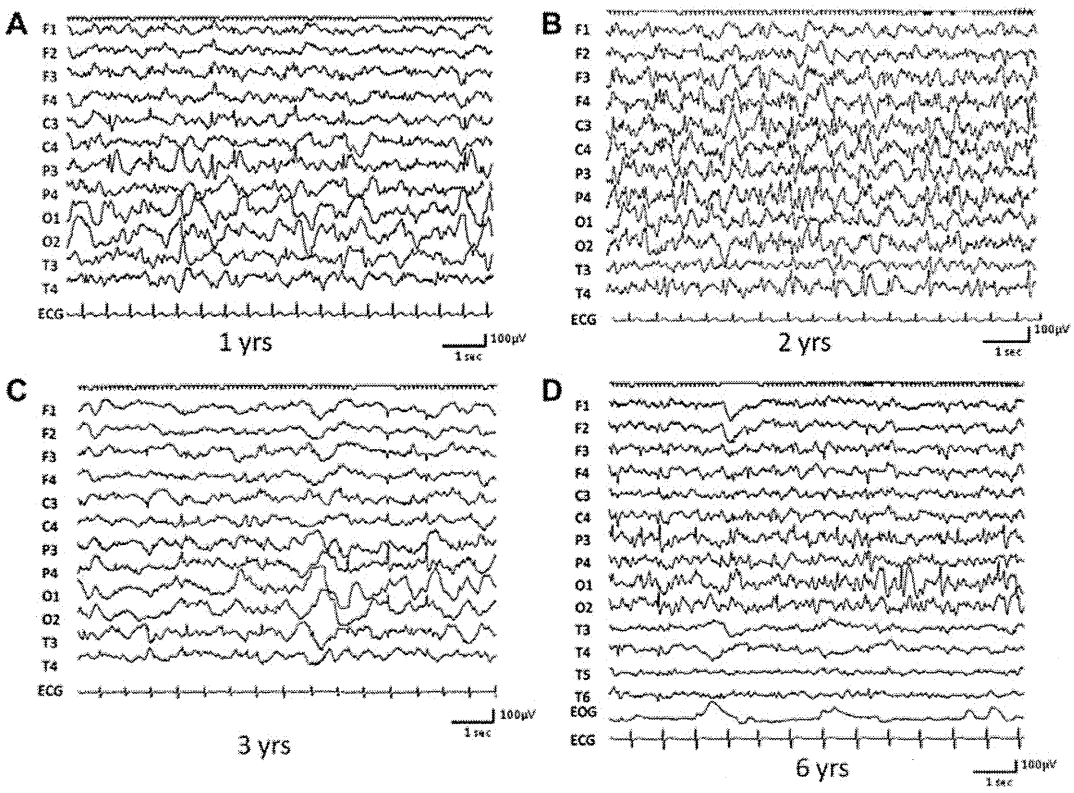

Fig. 2. Interictal EEG recordings of the patient. Interictal EEG data revealed multifocal spikes at the P3 and T4 areas at age 1 year (A), at C3–T3 and P4–T4 at age 2 years (B), at T3 and P4 at age 3 years, and at P3–O1 and O2 at age 6 years (D). The multiple spikes were tri-phasic in shape, similar to rolandic spikes.

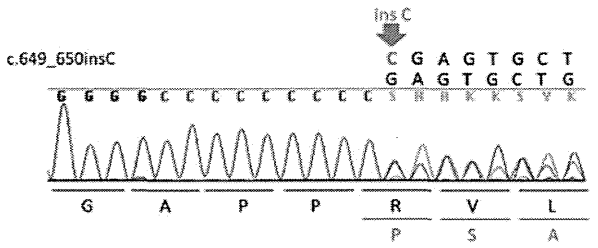

Fig. 3. Direct sequencing analysis of the proband (II-1) reveals a heterozygous mutation of *PRRT2*: c.649_650insC. The insertion of C at position 649 changed the reading frame, resulting in the production of an altered protein.

similarity between the current patient's epilepsy and BIS (i.e., family history of seizures, normal development prior to onset, no underlying disorders or neurologic abnormalities, partial seizures [e.g., psychomotor arrest], and a normal developmental outcome), she presented with some features that differ from most patients with BIS. Most notably, the patient had persistent spikes on interictal EEG, which differs with respect to the location and chronologic course of spike discharges, from both patients with BIS and those with BIMSE. In particular, in the current patient, the spikes moved transiently to the occipital area and began to resemble the rolandic spikes recognized in benign childhood epilepsy with centrotemporal spikes and Panayiotopoulos syndrome. Hence, it is possible that the current patient incidentally has the pathological background of benign childhood epilepsy. However, this background remains to be fully understood. Genetic investigations of the effects of *PRRT2* mutation on idiopathic childhood-onset seizures or epilepsy may help elucidate the association between PRRT2-related pathology and the epileptic background of benign childhood epilepsy.

Acknowledgments

This work was supported in part by a Grant-in-Aid for Scientific Research from the Ministry of Education, Culture, Sports, Science and Technology of Japan.

References

[1] Fukuyama Y. Borderland of epilepsy, with special reference to febrile convulsions and so-called infantile convulsions (in Japanese). Seishin Igaku (Tokyo) 1963;5:211–23.

[2] Watanabe K, Yamamoto N, Negoro T, Takaesu E, Aso K, Furune S, et al. Benign complex partial epilepsies in infancy. Pediatr Neurol 1987;3:208–11.

Please cite this article in press as: Torisu H et al. Girl with a *PRRT2* mutation and infantile focal epilepsy with bilateral spikes. Brain Dev (2013), http://dx.doi.org/10.1016/j.braindev.2013.05.009

[3] Vigevano F, Fusco L, Di Capua M, Ricci S, Sebastianelli R, Lucchini P. Benign infantile familial convulsions. Eur J Pediatr 1992;151:608–12.
[4] Capovilla G, Beccaria F, Montagnini A. 'Benign focal epilepsy in infancy with vertex spikes and waves during sleep'. Delineation of the syndrome and recalling as 'benign infantile focal epilepsy with midline spikes and waves during sleep' (BIMSE). Brain Dev 2006;28:85–91.
[5] Chen WJ, Lin Y, Xiong ZQ, Wei W, Ni W, Tan GH, et al. Exome sequencing identifies truncating mutations in PRRT2 that cause paroxysmal kinesigenic dyskinesia. Nat Genet 2011;43:1252–5.
[6] Heron SE, Grinton BE, Kivity S, Afawi Z, Zuberi SM, Hughes JN, et al. PRRT2 mutations cause benign familial infantile epilepsy and infantile convulsions with choreoathetosis syndrome. Am J Hum Genet 2012;90:152–60.
[7] Marini C, Conti V, Mei D, Battaglia D, Lettori D, Losito E , et al. PRRT2 mutations in familial infantile seizures, paroxysmal dyskinesia, and hemiplegic migraine. Neurology 2012;79: 2109–14.
[8] Lee HY, Huang Y, Bruneau N, Roll P, Roberson ED, Hermann M, et al. Mutations in the gene PRRT2 cause paroxysmal kinesigenic dyskinesia with infantile convulsions. Cell Rep 2012;1:2–12.
[9] Ono S, Yoshiura K, Kinoshita A, Kikuchi T, Nakane Y, Kato N, et al. Mutations in PRRT2 responsible for paroxysmal kinesigenic dyskinesias also cause benign familial infantile convulsions. J Hum Genet 2012;57:338–41.
[10] Schubert J, Paravidino R, Becker F, Berger A, Bebek N, Bianchi A, et al. PRRT2 mutations are the major cause of benign familial infantile seizures. Hum Mutat 2012;33:1439–43.

Please cite this article in press as: Torisu H et al. Girl with a *PRRT2* mutation and infantile focal epilepsy with bilateral spikes. Brain Dev (2013), http://dx.doi.org/10.1016/j.braindev.2013.05.009

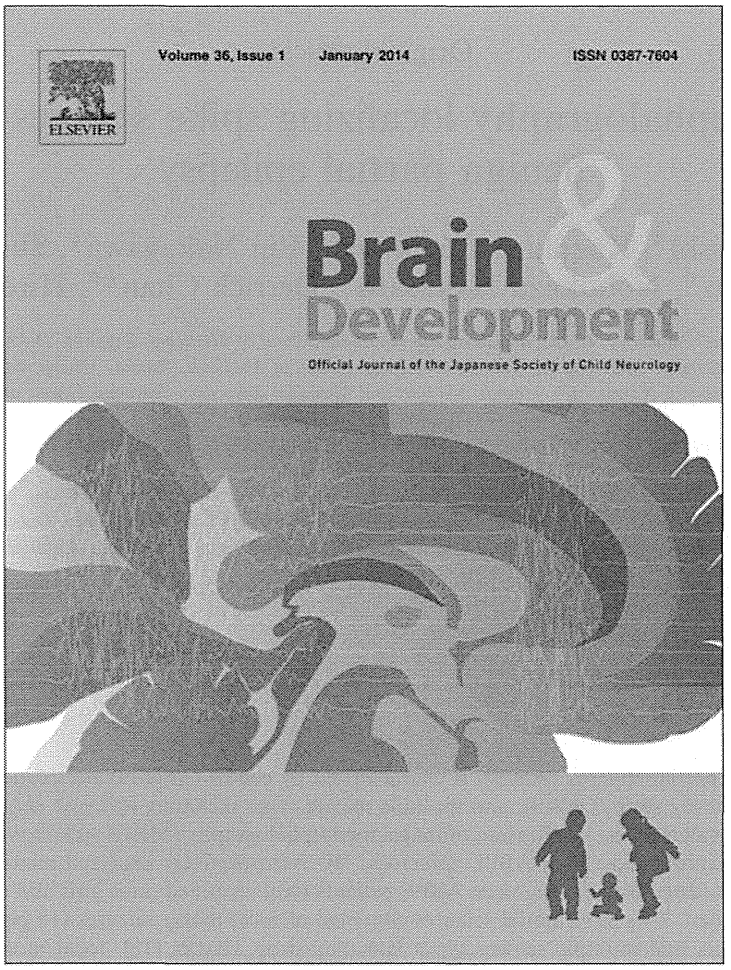

ELSEVIER

Brain & Development 36 (2014) 21–27

BRAIN & DEVELOPMENT
Official Journal of the Japanese Society of Child Neurology

www.elsevier.com/locate/braindev

Original article

Magnetoencephalography localizing spike sources of atypical benign partial epilepsy

Hideaki Shiraishi [a], Kazuhiro Haginoya [b], Eiji Nakagawa [c], Shinji Saitoh [a], Yutaka Kaneko [d], Nobukazu Nakasato [e], Derrick Chan [f,g], Hiroshi Otsubo [f,*]

[a] *Department of Pediatrics, Hokkaido University Graduate School of Medicine, Sapporo, Hokkaido, Japan*
[b] *Department of Pediatrics, Tohoku University School of Medicine, Sendai, Miyagi, Japan*
[c] *Department of Neurology, National Hospital for Mental, Nervous and Muscular Disorders, National Center of Neurology and Psychiatry, Kodaira, Tokyo, Japan*
[d] *Department of Neurosurgery, National Hospital for Mental, Nervous and Muscular Disorders, National Center of Neurology and Psychiatry, Kodaira, Tokyo, Japan*
[e] *Department of Epileptology, Tohoku University School of Medicine, Sendai, Miyagi, Japan*
[f] *Division of Neurology, The Hospital for Sick Children, University of Toronto, Toronto, Ontario, Canada*
[g] *Neurology Service, Department of Pediatric Medicine, KK Women's and Children's Hospital, Singapore*

Received 25 September 2012; received in revised form 24 December 2012; accepted 25 December 2012

Abstract

Rationale: Atypical benign partial epilepsy (ABPE) is characterized by centro-temporal electroencephalography (EEG) spikes, continuous spike and waves during sleep (CSWS), and multiple seizure types including epileptic negative myoclonus (ENM), but not tonic seizures. This study evaluated the localization of magnetoencephalography (MEG) spike sources (MEGSSs) to investigate the clinical features and mechanism underlying ABPE. *Methods:* We retrospectively analyzed seizure profiles, scalp video EEG (VEEG) and MEG in ABPE patients. *Results:* Eighteen ABPE patients were identified (nine girls and nine boys). Seizure onset ranged from 1.3 to 8.8 years (median, 2.9 years). Initial seizures consisted of focal motor seizures (15 patients) and absences/atypical absences (3). Seventeen patients had multiple seizure types including drop attacks (16), focal motor seizures (16), ENM (14), absences/atypical absences (11) and focal myoclonic seizures (10). VEEG showed centro-temporal spikes and CSWS in all patients. Magnetic resonance imaging (MRI) was reported as normal in all patients. MEGSSs were localized over the following regions: both Rolandic and sylvian (8), peri-sylvian (5), peri-Rolandic (4), parieto-occipital (1), bilateral (10) and unilateral (8). All patients were on more than two antiepileptic medications. ENM and absences/atypical absences were controlled in 14 patients treated with adjunctive ethosuximide. *Conclusion:* MEG localized the source of centro-temporal spikes and CSWS in the Rolandic-sylvian regions. Centro-temporal spikes, Rolandic-sylvian spike sources and focal motor seizures are evidence that ABPE presents with Rolandic-sylvian onset seizures. ABPE is therefore a unique, age-related and localization-related epilepsy with a Rolandic-sylvian epileptic focus plus possible thalamo-cortical epileptic networks in the developing brain of children.

Keywords: Epileptic negative myoclonus; Focal seizure; Atypical absence; Centro-temporal spike; Continuous spike and waves during sleep; Secondary bilateral synchrony

* Corresponding author. Address: Division of Neurology, The Hospital for Sick Children, 555 University Avenue, University of Toronto, Toronto, ON, Canada M5G 1X8. Tel.: +1 416 813 6660; fax: +1 416 813 6334.
E-mail addresses: hiotsubo@rogers.com, hiroshi.otsubo@sickkids.ca (H. Otsubo).

0387-7604/$ - see front matter © 2013 The Japanese Society of Child Neurology. Published by Elsevier B.V. All rights reserved.
http://dx.doi.org/10.1016/j.braindev.2012.12.011

1. Introduction

Atypical benign partial epilepsy in childhood (ABPE) initially presents with the following signs and symptoms: (i) onset age of 2.5–6 years; (ii) multiple seizure types including focal motor, atypical absences and myoclonic-atonic seizures; (iii) electroencephalography (EEG) showing central and mid-temporal spikes and diffuse slow spike-wave activities during drowsiness or sleep; and (iv) normal development or mild mental retardation [1]. Despite multiple seizure types and slow spike and waves on EEG, ABPE is distinguished from Lennox–Gastaut syndrome by its characteristic spontaneous remission, lack of tonic seizures or developmental delay, and normal awake EEG background activity. Since hemi-convulsive seizures during sleep and contralateral/bilateral centro-temporal epileptiform discharges are present at the beginning, the electro-clinical findings of ABPE are indistinguishable from those of benign epilepsy with centro-temporal spikes (BECTS) [2–5]. BECTS is the most well-recognized, age-related idiopathic focal epilepsy with occasional epileptic seizures despite frequent centro-temporal spikes on EEG. In contrast, ABPE patients tend to develop atypical absences or myoclonic-atonic seizures during the course of their condition. Tovia et al. [6] showed that 0.5% of patients with BECTS were categorized as atypical variants, while Doose et al. [7] found that 29% of the relatives of ABPE patients had some abnormal activities on EEG. Finally, Gobbi et al. [8] reviewed several subtypes of idiopathic focal epilepsies to categorize ABPE as a "Rolandic epilepsy-related disorder"; these age-related epilepsies including ABPE and BECTS were attributed to a maturational continuum with different manifestations.

Epileptic negative myoclonus (ENM) is one of the characteristic seizure patterns in ABPE. Oguni et al. [6] analyzed the ictal EEG findings of ENM and demonstrated generalized, bilateral synchronous discharges, while ictal magnetoencephalography (MEG) of an ABPE patient showed that the spike sources of ENM were localized at the peri-sylvian region [7].

MEG is a relatively new clinical technique that uses superconducting quantum interference devices (SQUIDs) to measure and localize sources of extracranial magnetic fields generated by intraneuronal electric currents. Current MEG machines have a whole-head array of more than 100 sensors contained within a helmet-shaped Dewar, which effectively covers most of the brain surface. MEG has been increasingly used for localization of the epileptic zone and functional mapping in epilepsy patients. MEG in BECTS patients showed spike sources with an anterior–posterior oriented perpendicular to the Rolandic fissure [8,9]. No case series of ABPE have thus far used MEG to localize epileptic spike sources.

We conducted a multi-center study to collect clinical, EEG and MEG findings in ABPE patients, with MEG used to characterize the spike sources (MEGSSs) in ABPE. We hypothesize that the epileptic network in ABPE is localized in both the Rolandic-sylvian cortex and thalamo-cortical networks, based on their unique clinical and electrophysiological features.

2. Patients and methods

We collaborated with four institutions on this study: the Department of Pediatrics, Hokkaido University School of Medicine (HU); Department of Pediatrics, Tohoku University School of Medicine (TU); Department of Pediatrics, National Center of Neurology and Psychiatry (NCNP), Japan; and the Division of Neurology, The Hospital for Sick Children (HSC), Toronto, Ontario, Canada.

2.1. Patients

We studied 18 patients with ABPE (nine females and nine males). We diagnosed ABPE according to the triad of diagnostic criteria as follows: (1) focal motor seizures, absences/atypical absences, atonic seizures including ENM, myoclonic seizures and drop attacks described by parents; (2) EEG findings of central and middle temporal spikes and generalized slow spike-wave activity during drowsiness or sleep similar to continuous spike and slow waves during sleep (CSWS); (3) normal development or mild mental retardation during the clinical course.

2.2. EEG

Scalp video EEGs were recorded using the international 10-20 electrode placement system and electromyography (EMG) electrodes for bilateral deltoid muscles to capture ENM. Awake and sleep EEGs were recorded in all patients.

2.3. MEG and magnetic resonance imaging

Initial MEG studies were conducted at the onset of ENM. Seven patients had multiple MEG studies up to six times. Parents or guardians of all patients provided written informed consent for the MEG studies. MEG and EEG were done in a magnetically shielded room. MEG was recorded using a system with 306 SQUIDs (Vectorview; Elekta-Neuromag Ltd., Helsinki, Finland) at HU, NCNP and TU, and with an Omega system (151 channels, VSM MedTech Ltd., Port Coquitlam, BC, Canada) at HSC. MEG data were recorded with a band pass filter of 0.03–133 Hz at HU, NCNP and TU, and of 1–208 Hz at HSC. Sampling frequency was 400 Hz at HU, 600 Hz at NCNP and TU, and 625 Hz at HSC. EEGs were recorded using the international 10-20 system, with additional electrocardiogram (ECG)